Methods of Modifying Through-thickness Electrical Conductivity of CFRP for use in Structural Health Monitoring, and its Effect on Mechanical Properties - A Review

Methods of Modifying Through-thickness Electrical Conductivity of CFRP for use in Structural Health Monitoring, and its Effect on Mechanical Properties - A Review

SC Brown, C Robert, V Koutsos, D Ray*

School of Engineering, Institute for Materials and Processes, The University of Edinburgh, The King's Buildings, Edinburgh, EH9 3FB, United Kingdom

Abstract

As the use of carbon fibre reinforced polymers (CFRP) is continuing to increase in engineering applications, more functionalities will be required. Having an enhanced through-thickness electrical conductivity can be a useful functionality for CFRPs which will minimise their damage from lightning strikes, and will help in their real-time monitoring. For most modification methods there is an adverse effect on the manufacturing and the fibre volume fraction, which influence the mechanical properties of the resulting composites. Simultaneous improvement of multiple properties of CFRPs is difficult, and as such the ways in which different materials and processes improve properties of CFRPs need to be understood in depth. This review discusses research that attempts to improve the through-thickness electrical conductivity of CFRPs with interest in the effects on mechanical properties, specifically interlaminar fracture toughness. The last section discusses the effect and use of these methods to improve structural health monitoring (SHM) of CFRP.

Keywords: Carbon fibre, Layered structures, Electrical properties, Fracture toughness, Thermosetting resin

1. Introduction

Carbon fibre reinforced polymers (CFRP) are being used increasingly in many applications. Their high specific strength makes them ideal for the automotive and aerospace industries. Despite having good mechanical properties, CFRPs exhibit some limitations. CFRPs with thermoset matrices are generally brittle in nature and are susceptible to impact damage [1, 2]. In addition to this, they have low off-axis electrical conductivity, herein referred to as conductivity, which can lead to joule heating and subsequent damage when current flows through the CFRP [3–19]. This review discusses the research carried out to enhance the through-thickness electrical conductivity, with consideration of the effect on mechanical properties. Some of the reported methods are not easily scalable to industrial levels, because they used either viscous resin mixes [20, 21], or complex processing techniques [9, 22]. Where possible the interlaminar shear strength (ILSS) and Mode I (G_{IC}) and Mode II (G_{IIC}) interlaminar fracture toughnesses are considered. Otherwise the measured mechanical properties are considered.

Carbon fibres themselves are highly conductive ($58.8\,\mathrm{kS\,m^{-1}}$ to $142.9\,\mathrm{kS\,m^{-1}}$) [23], but the matrix is electrically insulating in nature. This gives a high conductivity only along the fibre direction ($\approx 2\times10^{4}\,\mathrm{S\,m^{-1}}$), but the through-thickness conductivity is usually low ($10^{-3}\,\mathrm{S\,m^{-1}}$ to $10\,\mathrm{S\,m^{-1}}$) [24, 25] as the current flow is hindered in the resin rich regions. This limits the use of CFRPs in aircraft as the material needs to comply with safety standards for lightning strike protection (LSP) and electromagnetic interference shielding (EMI) [25–31].. To achieve these standards in aircraft currently, the carbon fibre composite is bonded to copper or aluminium mesh to produce a conductive outer-layer [32, 33]. This bonding often takes the form of adhering the metal to the CFRP surface with a resin layer, or adhesion of the metal to the CFRP surface using a glass fibre composite layer, ~~which also separates the CFRP and metal, reducing damage to the CFRP~~ which reduces galvanic corrosion between CFRP and the metal [34]. But this layer can be hard to apply, is not long-lasting, and increases the overall weight of the CFRP [9]. Novel solutions have been developed, such as a polyaniline/divinylbenzene layer [7], and cold metal spray coating methods [35] etc. [36].

Many different methods and materials have been used to improve the performance and through-thickness electrical conductivity of CFRPs. The methods used can be split into three categories: resin modification, the dispersion of a conductive material in the resin matrix, or the use of a conductive polymer resin; fibre surface modification, the grafting, growth, or chemical action on the carbon fibre surface to improve the conductivity of the fibre; and interleaving, the addition of conductive material between carbon fibre plies. The use of conductive through-thickness stitching by Rehbein et al. [8] was different to other reported techniques. All methods discussed in this review involve the addition of a third material to the CFRP using suitable techniques. The added materials are chosen for their specific properties e.g. nanoparticles for their large surface area, low weight and electrical conductivity. The addition of some of these materials creates problems, such as increased resin viscosity, poor fibre wetting, and weaker interfa-

*This document is the result of work funded by the ESPRC
*Corresponding Author
Email address: Dipa.Roy@ed.ac.uk (D Ray)

cial bonding. The method used to incorporate the materials into the CFRP is also an important consideration. Therefore this review discusses in detail the specific processes used to incorporate the conductive materials into the CFRPs. For example, Burkov et al. [20] reported that the degassing step of a carbon nanotube(CNT)/epoxy mix has a strong effect on the compressive toughness, showing how the process, not just the materials, are important to the final composite properties. The possible materials and methods are incredibly varied. As such, a large amount of future research will have to be done to understand all the mechanisms involved.

Given the much higher conductivity of carbon fibres compared to common matrix materials, the fibre volume fraction (FVF) is an important property to consider when discussing the electrical conductivity of CFRP. The effect of FVF on the conductivity is discussed in section 3, along with figure 17 which shows the variation of through-thickness electrical conductivity with FVF. Increases in the FVF of CFRP are limited by the manufacturing processes, and the conductivity is also greatly affected by the layup and consolidation of the final composite. The maximum achieved through-thickness electrical conductivity measured for a CF/epoxy baseline composite was $30.3\,\mathrm{S\,m^{-1}}$ at a FVF of $65.9\,\%$ [25].

The required conductivity of the the resulting CFRP is dependant on the desired functionality. A lower electrical conductivity helps in higher damage detection in composites through resistance sensing. But with higher electrical conductivity, the damage detection sensitivity is reduced [37]. This reduction is due to the addition of more percolating paths, meaning the bulk conductivity is affected less by damage and defects. Whereas for lightning strike protection and EMI shielding, a maximised conductivity is desired, this reduces damage by dissipating the lightning current [31, 33, 34, 38] well and acts as a better EMI shield [4]. Damage detection and lightning strike protection are both discussed below as examples, with damage detection expanded on further in section 4 due to its wide ranging applications.

An increase in electrical conductivity has been used to detect damage in the internal structure of the composites [39–44]. Work has been done adding CNT to glass fibre reinforced polymer (GFRP) matrices to produce conductive paths which allow for damage detection through voltage measurements [45, 46]. Other methods, such as fibre surface modification in the form of growth and deposition of nanoparticles, have also been used to enhance the through-thickness electrical conductivity of CFRPs [22, 47, 48]. The enhanced conductivity is strongly affected by the interfacial debonding at the fibre/matrix interface, as the conductive path is broken, as discussed in section 4 [40, 49]. Interleaves have also been used in GFRPs to detect real time fatigue crack growth [50]. Damage detection in unmodified CFRPs has also been done, and shows promising results [40, 51]. Schueler et al. [40] used electrical conductivity mapping to detect damage in CFRPs. Kim [37] showed that the crack detection is possible in CFRPs with CNTs grown on the carbon fibre surface. The surface modified CFRPs showed a larger change in conductivity with crack growth than the unmodified fibre samples, shown in figure 1.

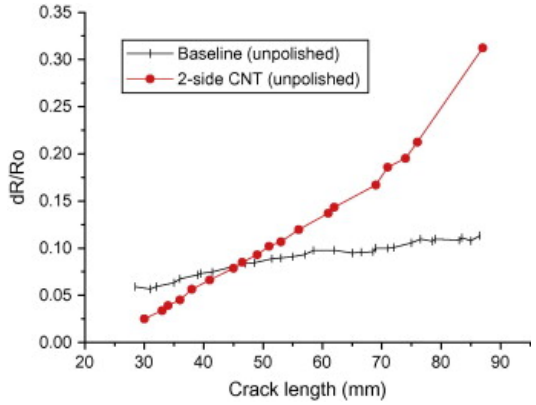

Figure 1: Comparison of resistance change between baeline and two-sided CNT sample. Used with permission [37]

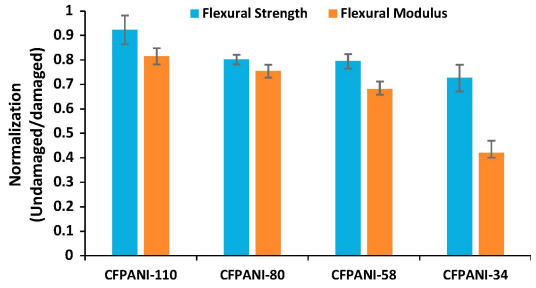

Figure 2: Comparison of damaged areas using non-destructive imaging and actual damaged area for PANI based composites with different through-thickness conductivities [33]

LSP requires maximising the electrical conductivity of the CFRP. Work by Kumar et al. [33] shows that the area damaged by a simulated lightning strike is greatly reduced in more conductive CFRPS. As shown in figure 2, the mechanical properties see the smallest loss of strength after simulated lightning strikes, with the loss of strength increasing with decreasing through thickness conductivity.

In addition, when high performing structural components, such as in aircraft, are made conductive by various modification techniques, it is important to consider the balance of conductivity and structural performance such as interlaminar fracture toughness; whilst for sensing, the structural performance is less critical. CFRPs have very good in-plane mechanical properties such as tensile and compressive strength. But they have poor resistance to interlaminar fracture. The interlaminar fracture toughness of a CFRP is affected by many different factors, including lay-up configuration, fabrication quality and procedure, specimen thickness, and environmental effects [52]. There are multiple methods for improving the interlaminar fracture toughness beyond optimization of production methods [52]. Some of the techniques used to improve interlaminar fracture toughness show great similarities to those used to improve through-thickness electrical conductivity, whilst others can be adapted to simultaneously improve both the properties, which is desirable.

2. Methods for Improving the Through-thickness Electrical Conductivity of CFRPs

2.1. Resin Modification

The mixing of conductive filler with the liquid resin before infusion improves the conductivity whilst also influencing the mechanical properties. CNTs are a common way to improve the conductive properties and are preferred due to their low density and one-dimensionality [53]; which leads to a low percolation threshold ($<1\,\%$), as discussed further in section 3 [54–56]. The conductivity is improved by modifying the resin to achieve percolation of the filler, this creates a conductive path through the insulating resin increasing the conductivity by up to nine orders of magnitude [56]. One of the main problems with CNTs (and other nanofillers) is their dispersion; they have a tendency to agglomerate leading to a non-uniform dispersion. The tendency of nanoparticles to agglomerate is a result of their high affinity for each other and lower affinity for the resin, which creates high surface tension. This is partially solved using different mixing methods, such as sonication, extrusion or shear-mixing of the filler within the epoxy resin [20, 55–57]. The addition of fillers to the resin increases the resin viscosity to a significant extent which makes the fibre wetting difficult leading to voids [20]. The poor wetting is mitigated by using a slow infusion method which gives more time for wetting to occur, but this can become unreasonable for high filler contents, as the viscosity and hence the required wetting time becomes too long. Voids can be removed by degassing the resin before infusion.

Burkov and Eremin [20] manufactured CFRP laminates with carbon twill fabrics (fiber Tenax ®HTA 40/200 tex, 3k) , basalt fabrics (VATI), and Bisphenol-F epoxy resin (Poxysystems ®epoxy L). The fibres were layed up as $[(0/90_C)_4, (0/90_B)_2]_s$ to produce an orthotropic laminate. The basalt layers were added to reduce the contact between carbon fibres to more directly investigate the effect of the CNT dispersion on the through-thickness electrical conductivity. Single walled carbon nanotubes (SWCNT) were added to the resin before curing and ultrasonication was performed for $20\,\mathrm{min}$ at $22\,\mathrm{kHz}$ and $130\,\mathrm{W}$. The epoxy resin was then hand mixed with the hardener. CNT contents of $0\,\mathrm{wt}\%$, $0.1\,\mathrm{wt}\%$, $0.2\,\mathrm{wt}\%$, and $0.3\,\mathrm{wt}\%$ were used. No degassing was done for the $0.1\,\mathrm{wt}\%$ and $0.2\,\mathrm{wt}\%$ CNT loaded laminates, which led to higher porosity in the samples resulting in a significant reduction of the compressive strength as shown in figure 3.

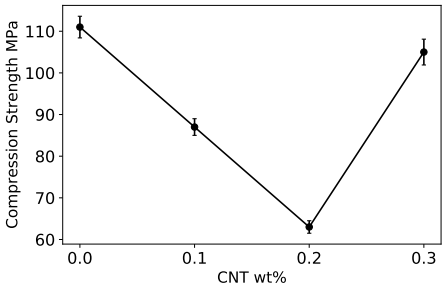

Figure 3: Variation of compressive strength of CFRP as a function of CNT loading. Reproduced with data from Burkov et al. [20].

Figure 4 shows SEM images of the crack surfaces, figure (a) is clearly more porous than figure (b) due to the degassing. Table 1 shows the through-thickness electrical conductivity values (σ_z) alongside the CNT loading, the flexural strength, and ultimate tensile strength. The conductivity measurements were taken by coating both surfaces with silver conductive paint and then measuring the resistance with an LCR meter. As shown in table 1, the entrapped air and resulting porosity does not affect the ultimate tensile strength or flexural strength significantly. This is because the tensile strength is taken up by the fibres with the voids having little effect.

Sawi et al. [21] introduced double walled carbon nanotubes (DWCNT) into a composite that consisted of UD carbon fibres (Toray T700S) in a Epoxy Resin (RTM6 Hexcel Coporation). The DWCNTs were dispersed in water with the surfactant hexadecylamine using ultrasonication at room temperature followed by a strong sonication. The mixture was then stirred into the epoxy resin and degassed. The percolation threshold was achieved at around $0.04\,\mathrm{wt}\%$ CNT. To reach a high conductivity a content of $0.4\,\mathrm{wt}\%$ CNT was used. The toray

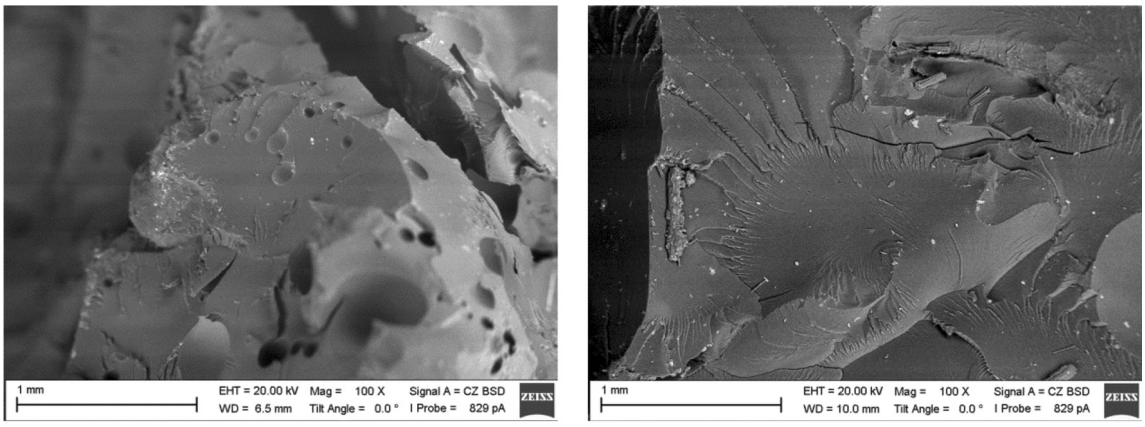

Figure 4: SEM images of epoxy fracture surface a) without (CNT-2) and b) with (CNT-3) degassing used with permission [20].

Table 1: Mechanical properties and through-thickness electrical conductivity (σ_z) of CFRPs loaded with different CNT contents[20].

Specimen	CNT (wt%)	Flexural strength (MPa)	Ultimate tensile strength (MPa)	σ_z ($\mathrm{S\,m^{-1}}$)
CNT-0	0	493.1 ± 1.7	601.7 ± 18.8	$< 10^{-5}$
CNT-1	0.1	510.4 ± 59	590.8 ± 13.5	7 ± 1.18
CNT-2	0.2	585.1 ± 58	583.5 ± 17.2	16.3 ± 1.02
CNT-3	0.3	604.9 ± 29	604.6 ± 15.3	66.2 ± 9.9

T700 carbon fibres were pre-impregnated with the epoxy resin mixture using resin film infusion. The impregnated individual UD plies were then stacked in a $[0]_8$ lay up sequence and cured in an autoclave. Two-point and four-point probe measurements were initially carried out, which revealed similar electrical conductivity values. Therefore two-point probe measurements were taken for subsequent samples. The conductivity increased from $0.0066\,\mathrm{S\,m^{-1}}$ to $0.53\,\mathrm{S\,m^{-1}}$ with the addition of $0.4\,\mathrm{wt}\%$ DWCNT. Measurements of the electrical conductivity were taken for a range of temperatures from $-150\,^{\circ}\mathrm{C}$ to $130\,^{\circ}\mathrm{C}$ with a $10\,^{\circ}\mathrm{C}$ step to investigate the temperature dependence of the CFRP. They showed that the through-thickness conductivity of the CFRP does vary with temperature. The conductivity of the sample was measured by recording the impedance using a Solartron-Schlumberger frequency response analyser with a Novocontrol interface. Silver paint was applied to the surface beforehand. The conductivity increased with increasing temperature for both the modified and unmodified epoxy CFRPs. The increase in conductivity with temperature is attributed to the partially semiconducting behaviour of the carbon fibres and CNTs, and the tunnelling effects between fibres and CNTs [58, 59].

Zhang et al. [25] mixed carbon black (CB) and copper chloride (CC) into the baseline composite consisted of UD carbon fibres (Toray T300J 6K) in bisphenol A epoxy resin (DGEBA, Huntsman Advanced Materials Ltd). The CB agglomerates were larger than the fibre separation, and would have been filtered out by the carbon fibres during resin infusion. To solve this an epoxy/CB masterbatch was prepared by planetary ball mill, which reduced the agglomerate size of the CB so that it was not filtered out. The masterbatch was then diluted to lower CB contents using more epoxy resin, and the copper chloride (CC, $CuCl_2$) was added to a concentration of $3 \times 10^{-6}\,\mathrm{mol\,g^{-1}}$ to the epoxy resin along with the hardener. The CFRPs were produced by vacuum assisted resin infusion (VARI) in two different layups ($[0]_{12}$ and $[0]_{24}$) for mode I and II type interlaminar fracture toughness tests. Once the resin infiltrated the fibres, the laminate was cured in a hot press to give a high fibre volume fraction of $65\,\%$. The bulk resistance was measured with a digital multimeter and the resistivity was calculated using the equation

$$\sigma = \frac{L}{RA} \tag{1}$$

where A is the cross sectional area, R is the volume resistance, and L is the length of the specimen. The dimensions A and L represent different geometrical dimensions of the specimen for the different measurement directions. The results of the conductivity and mechanical tests are shown in table 2. The improved conductivity was a result of the CB creating a conductive percolating network. The CC increased the tendency of the CB to form clusters, which lowered the percolation threshold of the CB as the tendency to form clusters meant that the CB were close enough to form conductive pathways. The small increases in the mode I and mode II interlaminar fracture toughness were attributed to the CB particles which increased the fracture surface area. The reasons for the increased clustering when CC is added could be excluded volume interactions, as this would cause the CB particles to attract, or the introduction of the CC ions screening the charged CB surface reducing the repulsive interaction [60, 61].

Table 2: Types Mode I (G_{IC}) and Mode II (G_{IIC}) interlaminar fracture toughness and through-thickness electrical conductivity (σ_z) of baseline CFRP and carbon black/copper chloride modified epoxy CFRP (CB/CC-CF) [25].

Sample	G_{IC} ($\mathrm{J\,m^{-2}}$)	G_{IIC} ($\mathrm{J\,m^{-2}}$)	σ_z ($\mathrm{S\,m^{-1}}$)
Baseline	974 ± 65	838 ± 133	30.3
CB/CC-CF	1415 ± 117	877 ± 144	55.6

Senis et al. [24] dispersed graphene oxide (GO) flakes within the epoxy resin matrix. The baselines composite consisted of UD Carbon fabric (Zoltek Panex 35) in epoxy resin (BASF Baxxores®ER 5300). GO was produced by the oxidation of graphite which formed hydroxyl and epoxide groups on the surface. These groups made the GO more compatible with the epoxy resin, improving the dispersion. The GO was dispersed into the epoxy matrix using high speed planetary mixing, which introduced high shear forces. VARI (vacuum assisted resin infusion) was used to infuse the fibres. The viscosity increased with increasing GO concentration. The DC resistance was measured using a two-probe system with an insulating frame as shown in figure 5.

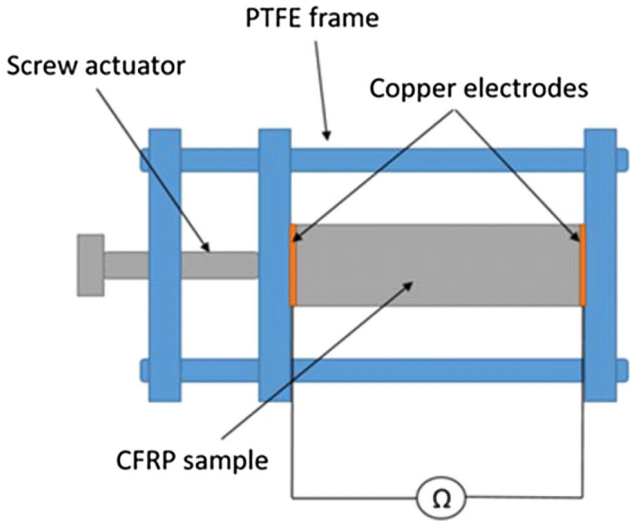

Figure 5: Diagram of the test fixture used for the electrical conductivity measurements used with permission. Used with permission [24].

A PTFE frame with a screw actuator was used to produce consistent contact between the measurement probes and the sample by applying pressure to the sample with two copper plates. The measurements were taken at a pressure of $5\,\mathrm{MPa}$, because above this pressure the resistance was unchanged. The surface of the composite was sanded to remove excess polymer and the exposed surface was coated with silver particles to reduce contact resistance for the electrical measurements. The composites showed improvements in both mechanical and electrical properties. The through-thickness electrical conductivity increased from $5.43\,\mathrm{S\,m^{-1}}$ to $18\,\mathrm{S\,m^{-1}}$ and, as shown in figure 6 , the interlaminar shear strength (ILSS) increased from $34\,\mathrm{MPa}$ to $50\,\mathrm{MPa}$ for the $0.63\,\mathrm{vol\%}$ GO composite. The ILSS reached a maximum value of $63\,\mathrm{MPa}$ for a GO volume fraction of $0.63\,\mathrm{vol\%}$. But this GO content had no effect on the through-thickness conductivity. The increase in the ILSS is attributed to the strong GO-matrix bonding and the GOs acting as crack deflectors, which impeded crack growth. The ILSS showed a noticeable drop between GO contents of $0.63\,\mathrm{vol\%}$ and $1.26\,\mathrm{vol\%}$ caused by reduced fibre wetting due to the higher

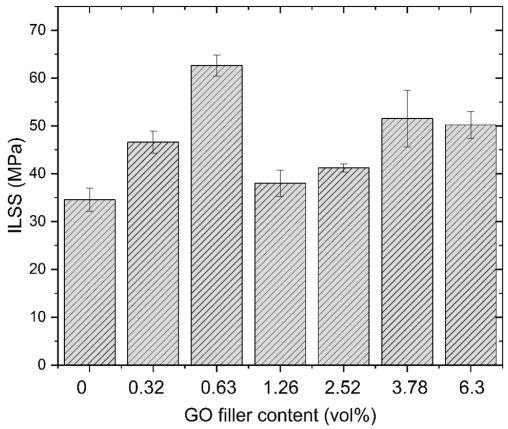

Figure 6: Graph of interlaminar shear strength of CFRP samples with increasing graphite oxide contents. Used with permission [24].

resin viscosity and increased agglomeration of the particles acting as defects. The ILSS began to increase again as the GO content was increased beyond $1.26\,\mathrm{vol\%}$ which might be due to the fact that the GO networks start acting as crack deflectors undergoing higher strain.

Zhao et al. [55] looked into the electromagnetic shielding of CNT modified CFRPs. The baseline composite consisted of UD carbon fibres (Toray 12K T700SC) in epoxy resin. The CNTs were dispersed in dichloroethane and mixed at different proportions with the resin. The resulting mix underwent ultrasonic mixing, was shear dispersed, dried to remove the solvent residue, and then mixed with the curing agent. The resin was rolled into films and then used to impregnate carbon fibre yarns by hot melt impregnation. As shown in table 3,

Table 3: ILSS and through-thickness electrical conductivity (σ_z) of composites produced by Zhao et al [55].

Sample	ILSS (MPa)	σ_z ($\mathrm{S\,m^{-1}}$)
Baseline	84.4 ± 2.1	0.16 ± 0.12
MWCNT-CFRP	98.8 ± 4.1	16.4 ± 9.1

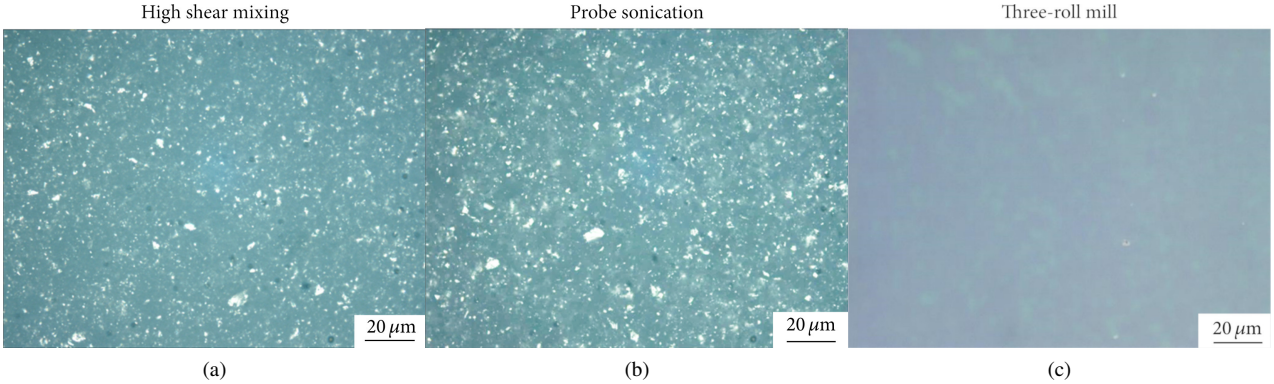

Figure 7: Optical microscope images of GnP dispersion samples for different dispersion methods. (a) high shear mixing (b) probe sonication, and (c) three roll milling [62].

both the ILSS and through-thickness conductivity were improved by the addition of CNTs. The increase in ILSS was attributed to bridging of the fibres.

Li et al. [62] used graphite nanoplatelet (GnP) modified epoxy resin to improve the properties of the baseline CFRP which consisted of carbon fibre fabric $[+45/-45/+45]$ (Toray T700) in epoxy resin (MVR444 Cytec Ltd.). The GnP was dispersed in the resin using three different methods; High shear mixing (HSM), probe sonication (PS), and three roll milling (TRM). Morphological analysis was performed on the pre-cured epoxy/GnP samples using an optical microscope to observe the level of GnP dispersion. Figure 7 shows that the best dispersion was achieved with the TRM dispersed GnP/epoxy mix. Only the electrical and mechanical properties of the CFRPs made from the TRM dispersed GnP/Epoxy were investigated. The final CFRP laminates were produced by VARI to produce samples of between $3.5\,\mathrm{mm}$ and $3.6\,\mathrm{mm}$ thickness, with $2\,\mathrm{wt}\%$ and $5\,\mathrm{wt}\%$ CNT loading. The through-thickness conductivity of the samples improved from $0.015\,\mathrm{S\,m^{-1}}$ to $0.6\,\mathrm{S\,m^{-1}}$ with the addition of $5\,\mathrm{wt}\%$ GnP. The ILSS and flexural modulus increased by $18\,\%$ and $13\,\%$ for the $2\,\mathrm{wt}\%$ and $5\,\mathrm{wt}\%$ samples respectively, which was attributed to GnP structures playing a positive role in crack deflection and crack bridging.

Kandare et al. [63] exploited dispersions of graphene nanoplatelets (GNP), silver nanoparticles (AgNP), and silver nanowires (AgNW) in epoxy resin used in carbon fibre/epoxy laminates. The baseline composite consisted of a plain weave carbon fabric (SigmaTex 199gsm, 2×2TW, 3k tow) with a bisphenol F epoxy resin (Renlam LY113). The graphene nanoplatelets were synthesized from graphite intercalation by heating the graphite to $700\,^{\circ}\mathrm{C}$, dispersing it in acetone and sonicating the mixture, to produce exfoliated GNPs. The mixture was then dried. AgNWs and GNPs were then dispersed in acetone and added to the epoxy resin. The acetone was then removed by mechanical mixing and thermal heating, and the mixture was ultrasonicated to disperse the nano-reinforcements. The mixtures were degassed. Six different modified epoxy samples were produced, which are outlined in table 5 with their through-thickness electrical conductivity, tensile and flexural strength values. The results show an increase for the through-thickness electrical conductivity, reaching a maximum value of $0.3\,\mathrm{S\,m^{-1}}$ with the addition of both GNPs and AgNWs with minimal effect on the mechanical properties. The AgNWs and AgNPs increased the conductivity more than the GNPs at lower concentrations. The AgNP showed the largest increase on their own with minimal effect on the mechanical properties.

Hirano et al. [64] produced polyaniline-based electrically conductive CFRPs. Conductive polymers such as polyaniline (PANI) are a possible alternative which when added produced electrically conductive CFRPs. There are a wide range of possible conductive polymers such as Polyacetylene, Polythiophene, Polypyrrole etc [65]. But polyaniline is often preferred for its good environmental stability, high conductivity, and cheaper and easier synthesis [66]. PANI-based composites were manufactured using a single-step process [67], which uses a PANI/DBSA(dodecylbenzenesulfonic acid)/DVB (divinylbenzene) blend to where DBSA acts as both a dopant for the PANI and a curing agent for the cross linking of the DVB. The final matrix system included PTSA(p-toluenesulfonic acid)to further improve the doping. Prepreg layers were prepared by impregnating plain woven carbon fibre with the PANI/DBSA/PTSA/DVB mix. The final composites were prepared as $[0/90]_8$, conventional CF/Epoxy composites were manufactured by with the same woven fibre and layup by VARTM (vacuum resin transfer moulding). To assess the effect of lightning strike damage, the flexural strength was measured before and after the application of simulated lightning currents. Table 4 shows the flexural strengths and through-thickness conductivities of the baseline CF/Epoxy composite and the conductive PANI/DVB composites. The PANI/DVB composites shows a much reduced flexural strength compared to the baseline. This was due to the weaker fibre/matrix interface in the PANI/DVB mix, which is caused by the sizing of the fibres being optimized for epoxy systems. The authors suggests that improving the sizing and mechanical properties of PANI based polymers would improve the mechanical properties. The greater conductivity

Table 4: Flexural Strength and through-thickness conductivity σ_z of baseline CF/Epoxy and CF/PANI/DVB composites [64]

Sample	Flexural strength (MPa)	σ_z ($\mathrm{S\,m^{-1}}$)
Baseline	610	2.7
PANI/DVB	267	74

Table 5: Composition, electrical and mechanical properties of the produced laminates with modified epoxy resin [63].

	Volume fraction %			Mechanical Strengths (MPa)			Electrical Conductivity
	GNP	AgNP	AgNW	Flexural	Tensile	Compressive	σ_z ($\mathrm{S\,m^{-1}}$)
CFRP	0	0	0	659 ± 13	665 ± 13	358 ± 15	0.077
CFRP/GNP	1	0	0	602 ± 55	679 ± 7	288 ± 15	0.17
CFRP/AgNP	0	0.05	0	647 ± 36	699 ± 0	348 ± 11	0.25
CFRP/AgNW	0	0	0.05	670 ± 18	573 ± 29	176 ± 20	0.2
CFRP/GNP/AgNP	0.95	0.05	0	601 ± 34	586 ± 4	322 ± 3	0.2
CFRP/GNP/AgNW	0.95	0	0.05	639 ± 39	633 ± 44	387 ± 25	0.3

in the PANI/DVB composite meant that after lightning strike it had a greater flexural strength than the epoxy based composite.

Kumar et al. [68] produced similar composites using a PANI-DBSA/DVB matrix. The matrix was manufactured by a two step process because it was found that in the absences of doped PANI, mixing DBSA and DVB resulted in an instantaneous exothermic reaction. PANI and DBSA were mixed at a ratio of $32.5\,\mathrm{wt}\%$ to $67.5\,\mathrm{wt}\%$ respectively, and then underwent thermally controlled semi-doping. The PANI-DBSA mix was then mixed at a $50:50$ ratio with DVB, and hand mixed to control the exothermic reaction. The PANI-DBSA/DVB matrix was used to hand layup 8 plies of carbon fabric which was subsequently cured in a hot press for $2\,\mathrm{h}$. The final samples were annealed separately for 5 different time periods, $2\,\mathrm{h}$, $4\,\mathrm{h}$, $6\,\mathrm{h}$, $8\,\mathrm{h}$ and $10\,\mathrm{h}$. Through-thickness electrical conductivity and flexural strength values are shown in table 6. The flexural strength increases with longer annealing time but seems to level out after $4\,\mathrm{h}$, this is attributed to the composite not being fully cured after the initial cure, after annealing for approximately $4\,\mathrm{h}$ the composite is completely cured. The flexural strength is lower than a typical CF/Epoxy composite, due to the weaker DBSA-PANI/DBV matrix. The through-thickness electrical conductivity decreases with annealing time which is attributed to the de-doping of the PANI.

Table 6: Flexural strength and through-thickness conductivity σ_z of DBSA-PANI/DVB composites [68]

Annealing Time (h)	Flexural Strength (MPa)	σ_z ($\mathrm{S\,m^{-1}}$)
2	238	135
4	289	115
6	333	103
8	346	90
10	No Data	83

2.2. *Fibre Surface Modification*

Another method used to improve the electrical and mechanical properties of CFRPs is fibre surface modification [69]. This involves the treatment of, or deposition onto, the carbon fibre surface. The aim of the modification is often to improve the interfacial interaction between the fibre and the matrix. The introduction of CNTs and GnPs on the surface introduces a conductive pathway that reaches much further past the fibre surface. The treatments used to create bonding groups on the fibre often introduce defects on the fibre surface, this weakens the fibre [70]. The deposition of additives on the carbon fibre surface can cause problems with reduced wetting of the fibre surface by the polymer as the additives create a high surface tension region around the fibre which the resin struggles to wet [71].

Pozegic et al. [22] grew CNTs on the carbon fibre surface at low temperature using photo-thermal chemical vapour deposition (PTCVD). This avoided damaging the surface and reducing the mechanical properties. The baseline composite consisted of 2/2 twill carbon fibre (Grafi Pyrofil TR30S) with two part epoxy resin (IN-2 epoxy infusion, East Composites$^{\mathrm{TM}}$). They did this by depositing $6\,\mathrm{nm}$ of iron as a catalyst on both sides of the woven fibre fabric surface using magnetron sputtering. Hydrogen was then introduced into the chamber at a pressure of $2\,\mathrm{Torr}$ ($\approx 266\,\mathrm{Pa}$) with $4\,\mathrm{kW}$ optical heating to reduce the iron oxide. Acetylene was added to the chamber and the growth process was performed on each side of the fibre twill. SEM results showed CNTs deposited on the surface of the fibre as shown in figure 8. The results showed an increase in the through-thickness conductivity of the final CFRP from $0.15\,\mathrm{S\,m^{-1}}$ to $0.7\,\mathrm{S\,m^{-1}}$. The conductivity was measured by painting the surfaces with silver and using a Keithley 4200 analyser by carrying out voltage sweeps from $-5\,\mathrm{V}$ to $+5\,\mathrm{V}$ with $0.1\,\mathrm{V}$ intervals.

Qin et al. [47] coated carbon fibres with GNPs by immersing them in a stable GNP suspension. The baseline composite consisted of UD PAN-based carbon fibres (unsized AS4 CF2

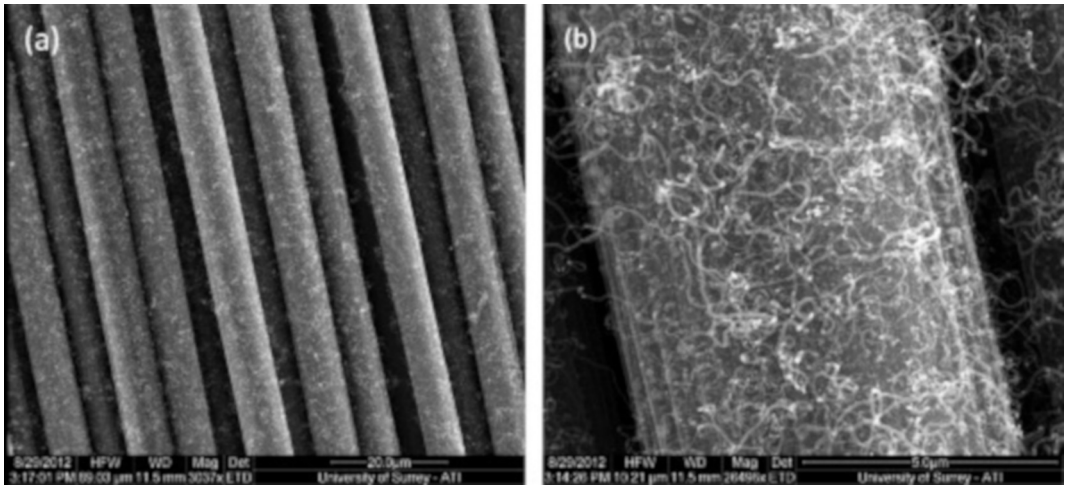

Figure 8: SEM images of (a) a bundle of carbon fibres following CNT growth (low magnification), (b) a single carbon fibre following CNT growth (high magnification). Used with permission [22].

12k, Hexcel Co.) with epoxy resin (Epon 828 Hexion Speciality chemicals). The fibres were pulled through the CNP suspension by rollers and then dried by passing them through heated tower shaped furnaces. Uncoated, epoxy sized, and GNP sized fibres were coated in resin using a drum-winder technique to produce unidirectional prepregs. The mechanical and electrical properties are shown in table 7. The epoxy and GNP sizing had little effect on the 0° flexural strength, but it improved the 90° flexural strength by 30 % and 47 % for the epoxy sized and GNP sized fibres respectively compared with the uncoated fibre laminates. The epoxy sizing had no affect on the through-thickness electrical conductivity, whereas the GNP sizing improved the conductivity from $2.5\,\mathrm{S\,m^{-1}}$ to $7\,\mathrm{S\,m^{-1}}$ for the uncoated and GNP coated fibre laminates respectively.

Table 7: Mechanical properties and through-thickness electrical conductivity (σ_z) of GNP coated fibre based composites [47]

	Flexural Strength (MPa)	ILSS (MPa)	σ_z ($\mathrm{S\,m^{-1}}$)
Baseline	1324 ± 57	64 ± 3	2.6 ± 1.0
Epoxy Coated	1324 ± 95	67 ± 5	2.4 ± 0.9
GNP Coated	1409 ± 123	78 ± 9	6.8 ± 1.4

Bhanuprakash et al. [48] manufactured CFRPs from graphene oxide coated carbon fibre fabric plies. The baseline composite consisted of UD carbon fabric (Hinfab HCU302) with Bisphenol-A based epoxy resin (Epofine-1564). Graphene oxide was synthesised by reacting graphite powder with a mixture of the strong oxidizing agents $NaNO_3$, H_2SO_4, and $KMnO_4$ which was then thermally exfoliated at 200 °C. Some of the exfoliated graphene oxide was then further reduced chemically using hydrazine hydrate to produce reduced exfoliated graphene oxide (rEGO). Carbon fibres were coated with the original GO (no reduction) by electropheretic deposition to produce GO-CF, some of the GO-CF was thermally reduced after the deposition to produce TrGO-CF. Carbon fibres were coated with the rEGO by a similar electropheretic deposition method to produce rEGO-CF. The a diagram of the electropheretic deposition setup is shown in figure 9. Table 8 shows the improvement in mode I interlaminar fracture toughness,

Table 8: Mechanical properties and through-thickness conductivity (σ_z) of the CFRPs produced. CF/EP has no graphene oxide, GO-CF/EP has graphene oxide coated fibres, TrGO-CF/EP has thermally reduced graphene oxide coated fibres, and rEGO-CF/EP has reduced exfoliated graphene oxide coated fibres [48].

Sample	ILSS (MPa)	G_{IC} ($\mathrm{J\,m^{-2}}$)	σ_z ($\mathrm{S\,m^{-1}}$)
CF/EP	31.3 ± 1.8	450.1 ± 26.6	13 ± 2
GO-CF/EP	46.1 ± 1.0	512.3 ± 28.7	22 ± 2
TrGO-CF/EP	45.1 ± 2.2	500.8 ± 24.8	31 ± 2
rEGO-CF/EP	44.2 ± 0.7	490.5 ± 33.6	26 ± 1

interlaminar shear strength, and through-thickness conductivity with the surface coating of the carbon fibres. The mechanical improvements were attributed to roughening of the fibre surface which created stronger mechanical bonding with the resin. The GO also had active functional groups ($-OH, -CO, -CO-$) which bonded with the resin. The lower interlaminar fracture toughness and interlaminar shear strengths for the rEGO-CF and TrGO-CF CFRPs was attributed to the removal of functional groups by the reduction. The increase in through-thickness electrical conductivity was attributed to the formation of a conductive layer of graphene oxide which produced effective conductive pathways between the carbon fibres. The higher conductivity values for the rEGO-CF and TrGO-CF fabric compared to the GO-CF fabric were attributed to the removal of the functional groups, giving the reduced GO a more pure, graphene-like structure.

Yan et al. [72] modified the surface of carbon fibres

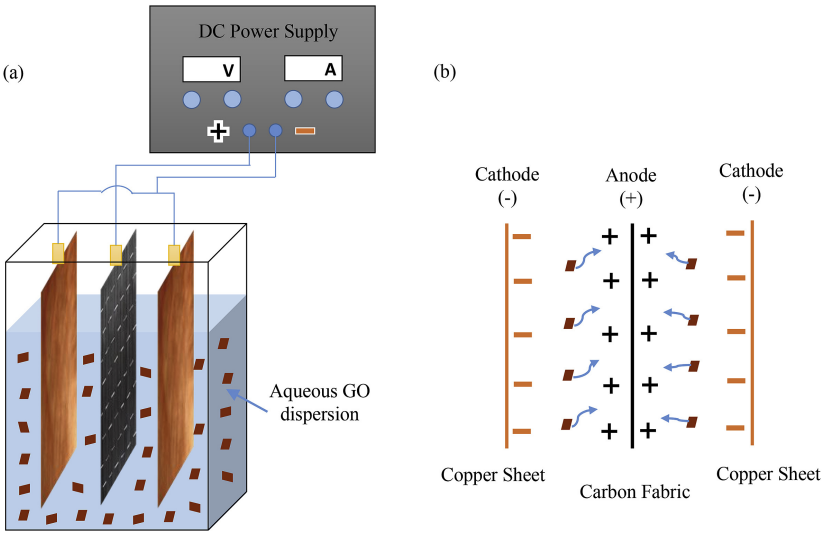

Figure 9: Schematic diagram of the electropheretic deposition technique used to coat carbon fibre plies (a) setup, (b) mechanism illustrating the deposition of graphene oxide. Used with permission [48].

with CNT and copper using both one-step and two-step electrophoretic deposition techniques. The baseline composite consisted of UD PAN-based carbon fibre (T300, 12K Sinosteel engineering Ltd) with epoxy resin (E-51, Nantong, Xingchen Company). The resulting laminates showed improved through-thickness electrical and thermal conductivity as well as higher ILSS. The fibres were soaked in acetone to remove the sizing. The one-step electrophoretic deposition was done with both positively and negatively charged CNTs. The positively charged method used $-NH_2$ modified CNTs with a positive copper plate anode and a carbon fibre cathode. The negatively charged deposition used $-COOH$ modified CNTs with a carbon fibre anode. Both techniques used copper compound electrolytes. For the two-step process, the copper was first coated on the fibres using electrophoretic deposition with a carbon fibre anode and copper cathode. Then steel plates were used as the cathode to allow for the deposition of CNTs onto the copper-CF surface. Tensile testing of the fibres showed that damage had occurred during the deposition reducing their tensile strengths. Large improvements in the ILSS and through-thickness electrical conductivity were observed as shown in table 9.

Table 9: ILSS and through-thickness electrical conductivity (σ_z) from Yan et al. [72].

Sample Name	Deposition Process	ILSS (MPa)	σ_z ($\mathrm{S\,m^{-1}}$)
Baseline	N/A	43.5	0.0065
CF0	Two-step Deposition	60.72	0.112
CF1	One-step Positive Deposition	58.5	0.186
CF2	One-step negative deposition	51.6	0.13

The resulting unidirectional laminates were then prepared using VARI. But the resulting laminates showed improvements in tensile strength of $34.5\,\%$ and $18.6\,\%$ for the positively and negatively charged depositions respectively.

2.3. Interleaving

Interleaving, the insertion of an additional layer between dry fibre reinforcements or prepreg layers, is a common way of improving both the interlaminar fracture toughness and the conductivity of CFRPs. Work has been carried out that considers both the through-thickness conductivity and the interlaminar fracture toughness, with some work succeeding in maintaining or improving the interlaminar fracture toughness whilst also improving the conductivity [4, 9, 73]. The work of Guo and Yi [36] gives a novel approach, with the use of AgNW coated paper interleaves as a means of conductivity improvement. Most of the work done has used polymer or carbon based interleaves. Interleaves can be easily incorporated into the manufacturing process. The introduction of extra layers reduces the fibre content and can adversely affect the mechanical properties

Guo and Yi [74] used conductive interleaves in CFRPs in the form of a flow-cast amorphous phenolphthalein poly(ether ketone) (PEK-C) thermoplastic interlayer coated with AgNW. The PEK-C was flow-cast into a thin film and perforated, the film was then dipped in a slurry of AgNWs. The AgNWs produced conductivity both across the film surface and through its thickness due to their presence at the hole edges. The films were interleaved between adjacent unidirectional CF/Epoxy prepreg layers and cured to produce the final composite. Table 10 shows that the addition of AgNW coated PEK-C interleaves improved the Mode I and Mode II interlaminar fracture toughness, but decreased the through-thickness conductivity of the CFRP. The work was done with the aim of improving both the conductivity and interlaminar toughness. The decrease in the conductivity due to the PEK-C interleave was partially mitigated with the AgNW coating of the PEK-C interleaves.

Table 10: Mechanical properties and through-thickness electrical conductivity (σ_z) of the baseline CFRP, the CFRP with a plain PEK-C interleave (PEK-C), and the CFRP with a AgNW coated PEK-C interleave (AgNW/PEK-C) [74].

Sample	G_{IC} ($\mathrm{J\,m^{-2}}$)	G_{IIC} ($\mathrm{J\,m^{-2}}$)	σ_z ($\mathrm{S\,m^{-1}}$)
Baseline	306	718	12.2
PEK-C	414 ± 33.5	1344 ± 20	0.0227
AgNW/PEK-C	396 ± 8.8	1576 ± 62	1.5

The use of (AgNW) loaded paper interleaves by Guo and Yi [36] produced results showing improved through-thickness electrical conductivity, but also reduced mechanical performance due to poor interfacial bonding. The baseline composite consisted of UD carbon fibre fabric (UC3160 CCF 300, 3K) with epoxy resin (3226 AVIC Composites Tehnology Co., Ltd). The interleaves were prepared by immersing paper ($11.26\,\mathrm{GSM}$, $16\,\mu\mathrm{m}$ to $18\,\mu\mathrm{m}$ thickness) into a slurry of AgNWs and then drying them in air at room temperature. This was done twice for the experimental samples. The interleaves were then placed one between each dry unidirectional carbon fibre ply in a $[0]_{24}$ layup, injected with resin, and cured. Table 11 shows the reductions by $77.4\,\%$ and $76.9\,\%$ for mode I and mode II interlaminar fracture toughness respectively, along with a through-thickness conductivity increase of $380\,\%$. The reduction in mechanical properties was attributed to the poor interface between the paper and the resin. The paper was too densely packed to allow any resin to permeate through, and there was no chemical bonding between the paper and the matrix. This suggested that the use of a more porous interleave, with better compatibility with the resin was required.

Table 11: Mechanical properties and through-thickness conductivity (σ_z) of the Baseline CFRP sample with no interleave and the CFRP with a AgNW paper interleave [36].

Sample	G_{IC} ($\mathrm{J\,m^{-2}}$)	G_{IIC} ($\mathrm{J\,m^{-2}}$)	σ_z ($\mathrm{S\,m^{-1}}$)
Baseline	321.1	1293	4.7
AgNW paper	104.8 ± 6.7	428 ± 19	17.9

Other work done by Guo et al. [73] used interleaves constructed from nylon and kevlar veils which were coated with Ag to improve the conductivity. The baseline composite consisted of UD CF/Epoxy prepreg (ACTC T800/5228). Veils are low density non woven fibre structures held together with some adhesive, they have a fibre volume fractions ranging from $30\,\%$ to $50\,\%$ with the remainder being mostly empty space. The nylon veils were made from long continuous nylon fibres, whereas the kevlar veils were made from randomly arranged chopped kevlar fibres. Both veils were coated by electroless Ag plating. To do this the veils were treated with diluted HCl and $SnCl_2$ and then activated by a solution of $PdCl_2$ and H_3BO_3, followed by reduction in NaH_2PO_2 solution. The veil was then plated using a solution of amino coordinated Ag salt and a solution of glucose as a reducing agent. The veil was removed after treatment and washed with deionized water. These last few steps with the Ag salts and washing were repeated at least three times. The veils were then dried in a vacuum oven at $45\,^{\circ}\mathrm{C}$. The CFRP consisted of CF/Epoxy prepregs laid up as $[0]_{24}$. Table 12 shows the improvement in both the mode I and mode II fracture toughness with the addition of the veil interleaves. The veil interleaves acted as crack bridges between

Table 12: Interlaminar toughness and through-thickness electrical conductivity (σ_z) of the baseline, uncoated (Pln), and coated (Ag) interleaves [73].

Sample	G_{IC} ($\mathrm{J\,m^{-2}}$)	G_{IIC} ($\mathrm{J\,m^{-2}}$)	σ_z ($\mathrm{S\,m^{-1}}$)
Baseline	306	718	12.2
Pln Nylon	666 ± 37	2410 ± 95	$< 10^{-6}$
Pln Kevlar	526 ± 23	1946 ± 57	–
Ag-Nylon	588 ± 52	2302 ± 79	$417 - 500$
Ag-Kevlar	420 ± 29	1652 ± 66	$345 - 500$

plies. The Ag plated interleaves had lower interlaminar fracture toughness than the plane nylon interleaves. The reduction in fracture toughness with Ag coating was attributed to a reduced surface interaction due to the Ag coating, and this was clearly evident in the SEM images where the crack was seen to propagate along the veil surface. But the Ag plated interleaves had a dramatically improved through-thickness electrical conductivity compared to the plain nylon interleaves. The resistivity of the samples were calculated by measuring the bulk resistance using copper plate electrodes and equation (1).

A comparison of work by Guo and Yi [36] and work by Guo et al. [73] is done to show the difference in the ability of the

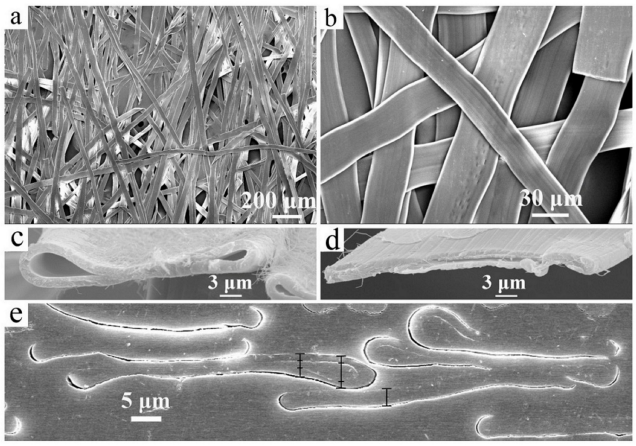

Figure 10: SEM images of (a,b) paper; (c,d) cross section of a plant fibre; (e) cross section of paper embedded in epoxy resin. Used with permission [36].

resin to infuse through different interleaving materials. Figure 10a shows an almost completely solid surface of paper fibres with no gaps to allow resin to permeate through. Whereas figure 11b shows a much less densely packed fibre veil surface, with gaps to allow resin to infuse. Table 13 shows that the nylon and kevlar had much lower volume fractions of veil fibre than the paper, which means there was more empty space for the resin to infuse into. The volume fraction and density was calculated

Table 13: Areal weight, density, and volume fraction of the paper, nylon, and kevlar veils [36]

Interleave	Areal weigth (GSM)	Density ($\mathrm{kg\,m^{-3}}$)	Veil Fibre Volume Fraction
Paper	11.26	625-704	0.42-0.47
Nylon	16.3	313	0.273
Kevlar	15.9	306	0.212

using the equation

$$VF = \frac{\rho_I}{\rho} = \frac{\rho_A}{T\rho} \tag{2}$$

here VF is the volume fraction, ρ_I is the interleave density, ρ_A is the areal density, T is the thickness, and ρ is the material density. The cellulose fibres also had a flattened structure rather than maintaining a cylindrical shape like the kevlar and nylon fibres which caused tighter packing. The compatibility of the epoxy and the interleave is also important, the kevlar and nylon are more compatible having more similar chemical groups and structure. This explanation does not take into account the differences in how the properties of the paper and the nylon/kevlar change with temperature. The cellulose, which makes up the majority of the paper interleave, maintains its strength and structure at higher temperatures. But the nylon and kevlar become more malleable as the temperature increases allowing the resin to infuse more easily into the polymer veil. Though an increase in malleability may also mean that the veil does not hold its structure and is therefore compacted reducing

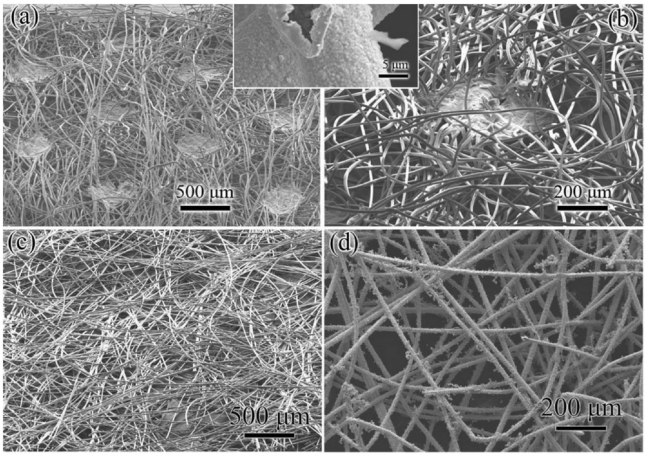

Figure 11: SEM images of the nylon veil $45°$ tilted away from horizontal plane: (a) Ag-plated, (b) plain, (Inset: one nylon fibre with broken silver coating), and Kevlar veil: (c) plain, $45°$, (d) silver-plated. Used with permission [73]

the space for infusion.

Li et al. [9, 75] used polyamide 12 (PA12) and multi-walled carbon nanotubes (MWCNT) to produce an interleave with strong interfacial bonding as well as good conductivity. The baseline composite consisted of high temperature UD CF/Epoxy prepreg (BONATECH Advanced Materials company). The surface of the interleave was plasma treated, producing reactive groups ($-COOH, -OH, -NHOC-, -NH$) to increase the number of chemical bonds at the surface. They also suggested that the plasma treatment played a second role by roughening the surface of the interleave, which was seen in the SEM images of the fractured samples. The roughening of the surface increases the surface topology which lead to crack deflection and creates more mechanical bonding. They produced their conductive thermoplastic films (CTF) by solution casting using DMF solvent mixed with MWCNTs. $1\,\mathrm{mm}$ diameter holes were drilled into the CTF to allow the resin to infuse, with 25 holes per square centimetre. The low temperature plasma treatment was done with oxygen, and figure 14 shows the different functional groups formed by the plasma treatment as well as their bonding with the epoxy resin. This bonding seems to play an important role in the interlaminar fracture toughness of the final CFRP. The CTFs were then interleaved with prepreg CFRPs in two different layups. A $[0]_{12}$ lay up with CTFs in between each prepreg was produced for conductivity testing, and a $[0]_{24}$ lay up with a CTF between the 12th and 13th prepreg for DCB testing [9]. A release agent coated PTFE film was also implanted between the 12th and 13th prepreg layers as a crack starter. The final laminates had different thicknesses, as the CTF had a thickness of $13\,\mu\mathrm{m}$ compared with the prepreg thickness of $0.13\,\mathrm{mm}$. The difference in the thickness need to be taken into consideration for accurate results. Both untreated and plasma treated interleaves were looked at, so that the effect of the plasma treatment on the conductivity and mechanical properties could be observed. The CNT content in the CTFs was also varied from $0\,\mathrm{wt}\%$ to $15\,\mathrm{wt}\%$ in $5\,\mathrm{wt}\%$ steps. Table 14 shows the different samples made with the codes used for their names. The results in figure 12 show lower mode I interlaminar fracture toughness for the untreated CTFs. This suggests that the interfacial bonding is much weaker without the plasma treatment and the subsequent chemical bonding. The results also show a relation between CNT content and improved mechanical properties for the plasma treated CTFs. This was attributed to an increase in the number of bridging CNTs being pulled out during crack propagation. The results for the electrical conductivity measurements show an increase in through-thickness conductivity for increasing CNT content, as shown in figure 13. There is also a slight increase in the through-thickness conductivity with plasma treatment. The increase in conductivity with CNT content was explained by the formation of more conductive pathways through the interleave. The increase due to the plasma treatment was caused by the increased roughness, which created a larger surface area on the CTF creating more conductive path connection to the CTF. The improvement in conductivity may have been limited by the plasma treatment reducing the conductivity of the CNTs at the surface by their oxidation. The conductivity of the samples were measured using a Keithley 6485 picoammeter. The samples were polished with abrasive paper, cleaned with acetone, allowed to dry, and then coated with a layer of conductive silver paste. The conductivity was calculated using equation (1).

Barjasteh et al. [76] produced conductive interleaves with graphene/graphite coated PA12 non-woven fabric of areal weights $6\,\mathrm{gsm}$ and $12\,\mathrm{gsm}$. The baseline composite consisted of UD stitched fibres (Toray T300) with benzoxazine based resin (Loctite BZ 9110 Aero). Two different coating methods were used to produce the interleave. The first involved rubbing a graphite sheet with the PA12 fabric to produce a graphite layer on the surface of the PA12. The second method used two immiscible solvents (hexane and water) to which graphite powder was added and the mixture was then sonicated. The PA12 fabric was then added and the mixture was sonicated again. After drying, the PA12 interleaves were placed between every two layers of stitched unidirectional carbon fabric. A thin graphite layer was produced at the interface of two immiscible liguids. The graphite layer then readily bonded by van der waals interactions to the PA12. The use of sonication allowed more accurate control of particle size than the rubbing method, which produced varied particle sizes. The conductivity of the fabrics, varied depending on the method used and the duration of the treatment i.e. if the fabric was rubbed for longer against the graphite it became more conductive. The final laminate was produced by VARTM. The resistance was measured using a Keithley 2400 whilst the CFRP was sandwiched between two copper plates. The conductivity was calculated using equation (1). The conductivity of the fabrics increased from essentially $0\,\mathrm{S\,m^{-1}}$ up to a value of $\approx 0.03\,\mathrm{S\,m^{-1}}$ at which point the rubbing method did not consistently increase the graphite content. Similarly the sonication time of the interfacial trapping method reached a maximum at around $4\,\mathrm{h}$ of sonication. The graphite particles were slowly broken down by the sonication, and for times longer than $4\,\mathrm{h}$ this breakdown became detrimental producing a decrease in the electrical conductivity. The through-thickness conductivity was improved in the CFRPs from less than $10^{-8}\,\mathrm{S\,m^{-1}}$ for the uncoated $6\,\mathrm{gsm}$ in-

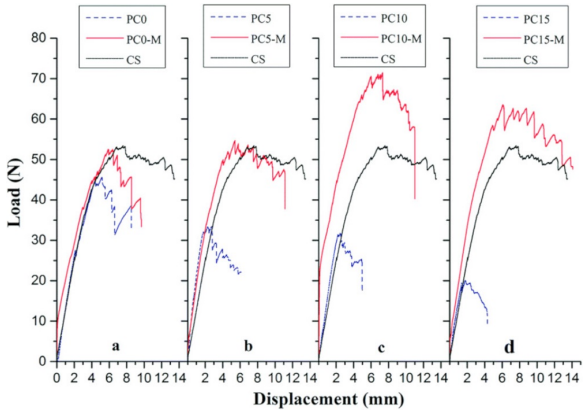

Figure 12: DCB load-displacement curves for different CFRPs. The codes for the final CFRP compositions are described in table 14, for the control (black), non-plasma-treated (dashed, blue), and the plasma-treated (red) samples, with increasing CNT content. Published by the Royal Society of Chemistry [9].

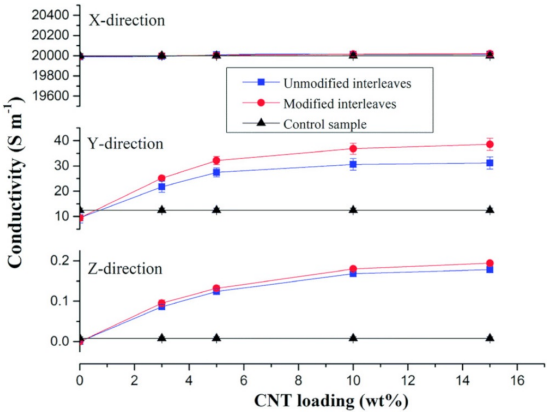

Figure 13: Results of conductivity measurements done by Li et al. [9] for the control (black) untreated (unmodified, blue), and plasma-treated (modified, black), for along fibre (X-direction), transverse (Y-direction) and through-thickness (Z-direction). Published by the royal society of chemistry [9].

terleave to $0.0025\,\mathrm{S\,m^{-1}}$ for the coated $6\,\mathrm{gsm}$ interleave. Table 15 shows the mode-I and mode-II interlaminar toughness values, there is noticeable improvement in both with the introduction of the PA12 interleaving veils.

Kumar et al. [4] used MWCNT buckypaper as an interleave between layers of prepreg, as well as on the surface of the composite. The baseline composite consisted of CF/Epoxy prepreg (F6343B-05P), with T300-3K fibres and epoxy resin(# 2500Toray Industries Inc.). Their work targeted improving the lightning resistance of the CFRP. Lightning strikes have a very high current which attempts to flow through the CFRP when struck. Joule heating is the process by which a current flowing through a resistive material heats that material. Joule heating is described by the equation

$$P \propto I^2 R \tag{3}$$

where P is the power, I is the current, and R is the resistance. Lightning strikes are very high current and produce a

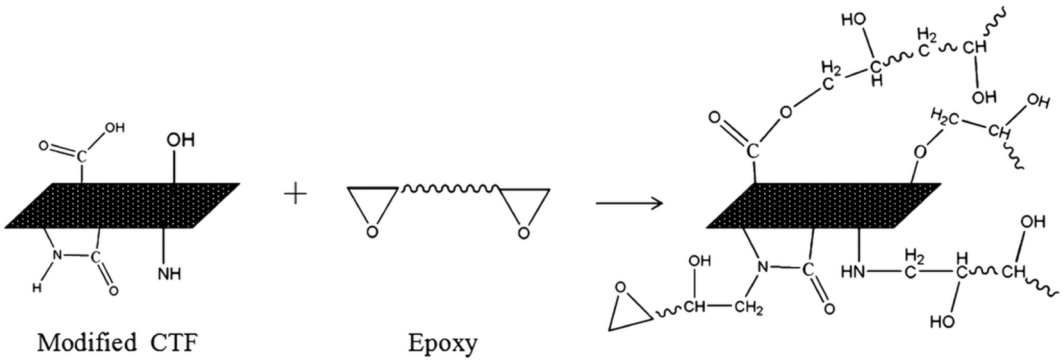

Figure 14: Image showing the groups formed by the plasma treatment and their bonding mechanisms with epoxy resin for the conductive thermoplastic interleaves (CTF). Published by the Royal Society of Chemistry [9].

Table 14: Different composites with different interleaves manufactured by Li et al. CS stands for control sample (baseline composite), PC are the interleaved samples. Published by the Royal Society of Chemistry [9].

Sample Code		Interleave	Fibre Volume Fraction (vol%)	MWCNTs Mass Fraction (wt%)
Without Plasma Treatment	With Plasma Treatment			
CS	–	–	63 ± 5	–
PC0	PC0-M	0 wt% MWCNTs/ PA12	62 ± 5	–
PC5	PC5-M	5 wt% MWCNTs/ PA12	62 ± 5	0.35
PC10	PC10-M	10 wt% MWCNTs/ PA12	62 ± 5	0.7
PC15	PC15-M	15 wt% MWCNTs/ PA12	62 ± 5	1.05

Table 15: Interlaminar shear strength properties of the baseline and graphite coated 12 gsm PA12 interleaved CFRPs. Used with permission [76].

Sample	G_{IC} ($\mathrm{J\,m^{-2}}$)	G_{IIC} ($\mathrm{J\,m^{-2}}$)
Baseline	273 ± 30	819 ± 73
Interleaved	388 ± 75	1941 ± 122

lot of power in the form of heat when they conduct through an object. By reducing the resistance, the power as heat is decreased. To produce the buckypaper, MWCNTs were oxidised at $375\,^{\circ}\mathrm{C}$ in air followed by the removal of impurities. The MWCNTs were filtered and washed with ethanol, and then left to cool in a vacuum oven to remove any moisture. MWCNTs were mixed with distilled water at $0.15\,\mathrm{wt}\%$ and with $1\,\mathrm{wt}\%$ ASE surfactant (blend of sodium linear alkylbenzenesulfonate and sodium lauryl ether sulphate). The mixture was then homogenized to form a uniform CNT suspension, which was ultrasonicated to break up any agglomerations. The buckypaper was produced by a vacuum filtering technique of MWCNT suspensions using a nylon mesh. The final product was $0.15\,\mathrm{mm}$ thick and was cut into plies. Four different samples were made, each with a different number of interleaves and different ply arrangements. Four prepreg layers were used with either resin interleave layers, buckypaper interleaves, or no interleave. The compositions of the four sample types are described in table 16. They showed that simple conductivity measurements are not necessarily an accurate prediction of the materials lightning strike protection. Their CFRPs showed an increase in through-thickness ~~and transverse~~ conductivity with increasing BP-layers, which was attributed to the conductivity of the buckypaper interleaves. The BP4-CF sample showed a noticeable drop in its mechanical properties, specifically the flexural strength. This was attributed to the buckypaper increasing the thickness of the CFRP and reducing the interlaminar bonding. They used imaging to characterise the lightning damage of their samples as shown in figure 15. They showed that the introduction of the conductive interleaves did reduce the visible lightning damage. Their data showed that the simulated lightning strikes did not decrease the flexural modulus and flexural strength of the more conductive samples as much. The lower resistance meant less heat was produced which decreased the amount of epoxy damaged by burning and vaporisation. But the more conductive samples had lower flexural moduli before the simulated lightning strike damage. The images in figure 15 show the visible damage caused by the simulated lightning strikes. The setup had the grounding at the edges of the panels, meaning that the current flowed outwards from the centre after the lightning strike. The two bottom samples have the buckypaper at the surface giving the darker colour. Figure 15 shows the difference in visible damage between (b), which had only a single layer of buckypaper on the surface, and (c), which also had buckypaper layers interleaved below the surface. The lower buckypaper layers were able to conduct away more current and heat reducing the damage done by the simulated lightning strikes further. The NDI (non-destructive imaging) images show reduced damage at the surface as a result of these extra conductive pathways. The small circular damage taken by NDI for BP0-CF is a result of the lack of dissipation of the heat or current heating and evaporating the epoxy at the lightning strike point. A comparison of the work of Kumar et al. [4] and the work of Hirano et al. [64], who used a different fibre, weave and epoxy, shows that the baseline composite is important as Hirano et al. observed greater after lightning strike damage in their baseline composite. This is an expected results as they are important factors in the conductivity of CFRPs. These parameters are already known to affect mechanical properties.

Table 16: Compositions of different interleaved CFRP samples [4]

Sample	Interlayer Structure
Baseline	3 additional epoxy interleave layers
BP0-CF	No interleaves
BP1-CF	1 BP on top of laminate
BP4-CF	3 BP layer interleaves and 1 BP layer on top

Zhao et al. [77] created chopped fibre interleaves by randomly dispersing the chopped fibre on a release film and coating the fibres in a $2.5\,\mathrm{wt}\%$ bismaleimide resin (BMI) wet film. The baseline composite consisted of carbon fibre (Toray 12K T700SC) with bismaleimide resin (9611 AVIC Composites Co. Ltd.).The results for electrical and compressive tests are shown in table 17. This increased the thickness of the interlaminar region meaning that for the thinnest layer $8\,\mathrm{gsm}$ the conductivity was increased to $27.9\,\mathrm{S\,m^{-1}}$. This interleaved CFRP also had weaker compressive strength due to the lack of resin in the interleave compared to the thicker samples.

Table 17: Compressive strength, ILSS, and through-thickness electrical conductivity (σ_z) of the baseline and 80 gsm interleaved sample [77].

Sample	Compressive Strength (MPa)	ILSS (MPa)	σ_z ($\mathrm{S\,m^{-1}}$)
Baseline	703-804	131	0.43
Interleaved	760	126	27.9

2.4. Other Methods

Rehbein et al. [8] used 3D stitching, a method which is commonly used to improve interlaminar fracture toughness in CFRPs. The baseline composites consisted of $(+45°, -45°)$ quasi-isotropic layups with 24K fibre tows in epoxy resin. Stitching is the process of using thread to stitch multiple layers of dry carbon fibre fabrics together in the through-thickness direction to allow for stronger interlaminar bonding. Stitching was also used in parallel with interleaving to improved the conductivity further producing mixed results. Stitching can damage the fibres [78], harming the mechanical properties by introducing defects and resin pockets. The stitching used silver coated polyamide yarns which have high linear conductivity (conduc-

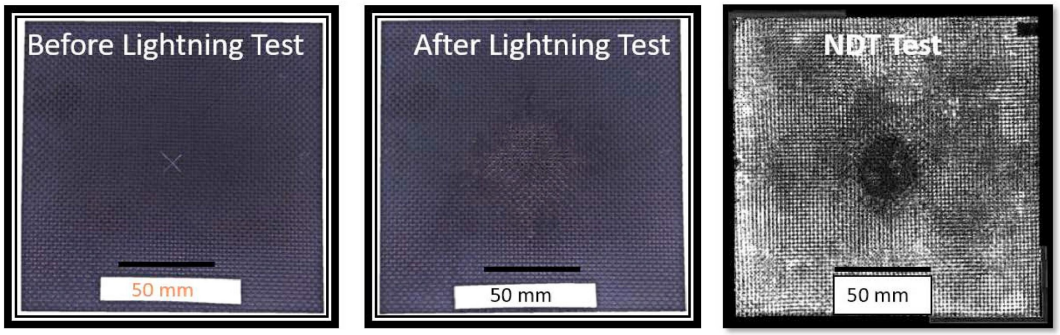

(a) BP0-CF

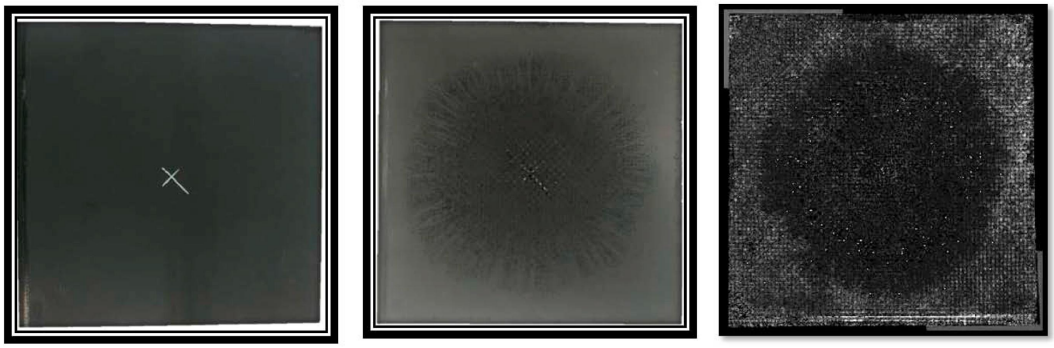

(b) BP1-CF

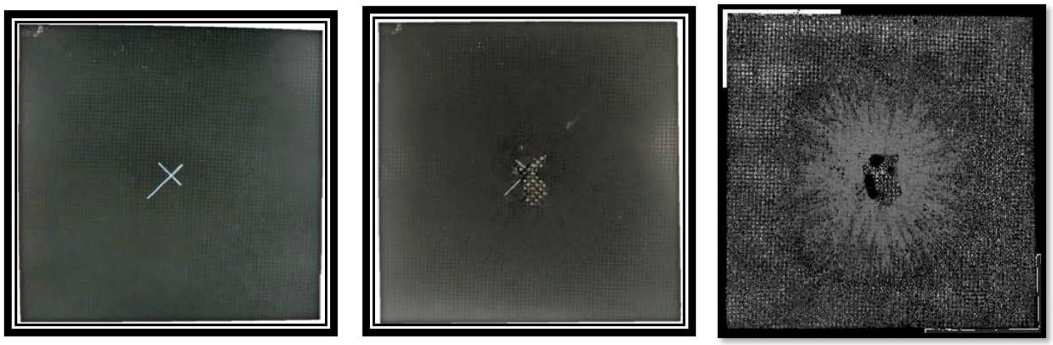

(c) BP4-CF

Figure 15: CFRP specimens before & after lightning strike and NDT images taken using a Scanning Acoustic Topograph connected to a 5MHz transducer (a) BP0-CF (b) BP10-CF and (c) BP4-CF. Used with permission [4].

Table 18: Yarn count, degree of silver coating, and linear resistance of nylon stitching yarns used. Used with permission [8].

Denomination	Yarn count (basic yarn)	degree of silver coating	Linear resistance	
			$\Omega\,\mathrm{cm}^{-1}$	Coef. of variation
33PL	33 dtex	very high	0.76	6.9 %
44PL	44 dtex	very high	0.63	12.4%
44HC	44 dtex	high	7.8	19.3%
110PL	110dtex	very high	0.29	10.3%

tivity per length) and flexibility. Using the stitching method described in figure 16

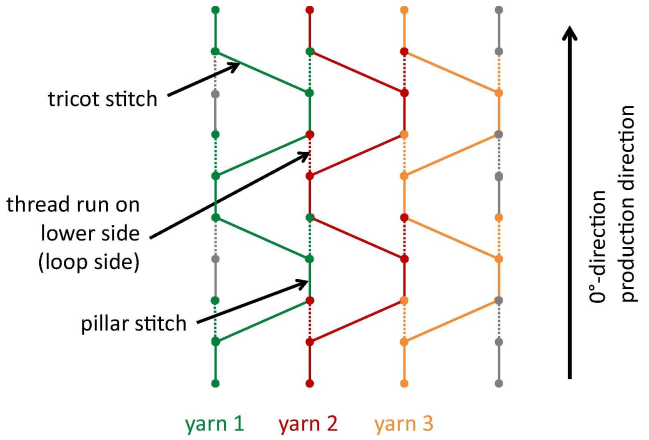

Figure 16: Knitting pattern of the silver coated polyamide, the tricot stitch refers to the stitch between the fibres and the pillar stitch is a winding or stitching around a single fibre. Used with permission [8].

the carbon fibres were stitched together to produce a single continuous structure. The fibres were oriented in a $+45°$ and $-45°$ direction for the non-interleaved samples. Previous work by them [79] has shown that the conductivity is decreased by approximately 40% when the fibre layers are parallel. The knitted yarns produced conductive routes between the fibres in the through-thickness direction. The laminates were then painted with epoxy paint, with the stitched-only laminates manufactured using VARI, and the interleaved samples manufactured by autoclave. Various silver coated yarns were used with different amounts of coating and different fibre counts, as described in table 18. The results of the through-thickness conductivity tests are shown in table 19. It was found that the introduction of these conductive stitching fibres produced CFRPs with conductivities of up to $627\,\mathrm{S\,m}^{-1}$, compared with only $5.0\,\mathrm{S\,m}^{-1}$ for the baseline composite. The yarn used also had an effect on the in-plane conductivity which showed a three-fold increase from $9956\,\mathrm{S\,m}^{-1}$ for the 44HC fibre to $30\,678\,\mathrm{S\,m}^{-1}$ for the 110PL fibre [8]. The bulk resistance was then measured and the resistivity was calculated using equation (1). Although no data was taken for the mechanical properties of the resulting CFRPs, other work on stitching showed improved interlaminar fracture toughness but also a decreased flexural strength in stitched CFRPs [80].

Table 19: Fibre volume fraction and through-thickness electrical conductivity (σ_z) of stitched and interleaved carbon fibres [8].

Yarn	FVF (%)	σ_z ($\mathrm{S\,m}^{-1}$)
	Baseline	
N/A	55.7	0.7
N/A	59.4	5.0
N/A	60.7	10.0
	Stitching Only	
33PL	54.5	170.1
44PL	53.9	245
44HC	54.5	26.6
110PL	50.3	627
	Interleaved Reference (No Stitching)	
N/A	53.7	18.2
	Stiching and Interleave	
33PL	54.8	335.7
44HC	54.8	103.4
110PL	51.4	571.8

3. Summary of Mechanisms of Conductivity Improvement

Conductivity in CFRPs is facilitated by the conductive carbon fibres, which are held in an electrically resistive polymer [81]. The conductivity of CFRPs is therefore dependent on the conductivity and the volume fraction of the fibres. Carbon fibres vary little in conductivity [23] , but the production method of the CFRP can affect conductivity, through voids, defects, and fibre volume fraction (FVF). Figure 17 shows FVF has a noticeable effect on the conductivity of the final composite. There is large variation in the conductivity of the samples, this is a result of differences in manufacturing processes. Figure 17 results show that a higher through-thickness conductivity is achievable with UD CFRPs, though this is likely a result of the ability of the fibres to pack better reaching higher fibre volume fractions.

Electrically conductive additives can be used to improve the electrical conductivity in the resin rich regions of CFRPs. If the concentration of additive is above the percolation threshold it increases the conductivity because a continuous conductive path is formed as in figure 18. The electrical conductivity increase can be roughly split into two regions. The first region

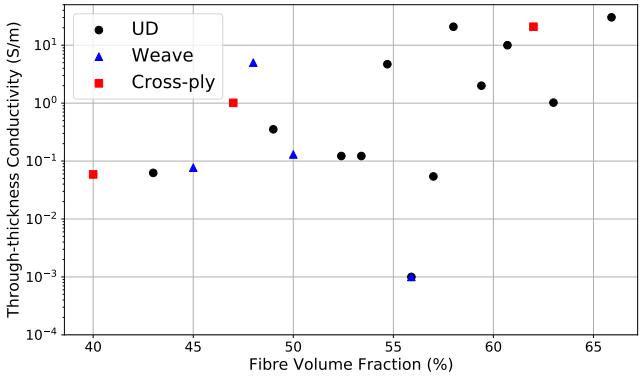

Figure 17: Graph of the variation of the through-thickness conductivity with the fibre volume fraction of the unmodified CFRPs. Data was taken from multiple papers that discuss through-thickness conductivity in Epoxy based CFRPS [4, 8, 9, 21, 22, 24–26, 36, 63, 72, 73, 76, 77, 82, 83]

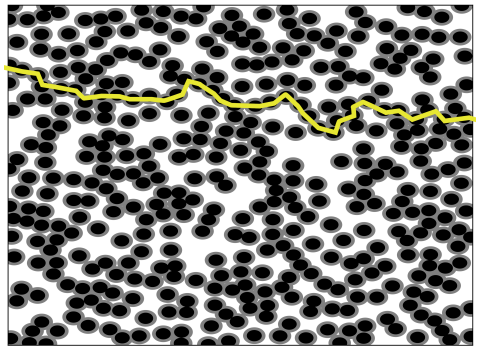

Figure 18: A schematic of low aspect ratio circular particles which have exceeded the percolation threshold

is below the percolation threshold where the conductivity increases as the additives increase because the additives creates partial paths with higher electrical conductivity than the matrix. The second region above the percolation threshold continues to show an increase, but at a much slower rate, in electrical conductivity with increasing additive concentration as more percolating paths are produced [20, 24, 25]. At low concentrations the circular particles do not produce a percolating network due to there minimal aspect ratio of 1, whereas the rods, which have a higher aspect ratio (20 to 1000), easily create a percolating network. Figure 19 is a schematic showing the percolation of high aspect ratio particles. It is possible to reduce the percolation threshold of particles by reducing the extent of the dispersion. Zhang et al. [25] reduced the percolation threshold of carbon black particles by increasing their agglomeration using copper chloride. Figure 20 is a schematic showing the percolation thresholds for CNTs with varying aspect ratios. The data shows that lower percolation thresholds are achieved for higher aspect ratios. Figure 20 also shows a large amount of variation in the percolation threshold for the same aspect ratio, which can be attributed to the different dispersion methods used. Computational models of the percolation of ellipsoids of varying aspect ratios supports this prediction as well, with work suggesting percolation on the order of $0.285\,\mathrm{vol}\%$ for a sphere,

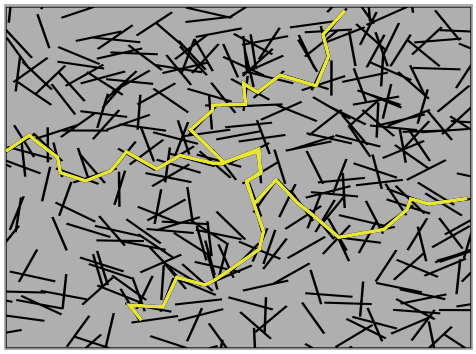

Figure 19: A schematic of percolation through a high aspect ration particle network.

and $0.001\,\mathrm{vol}\%$ for a prolate ellipsoid with an aspect ratio of 500 [84].

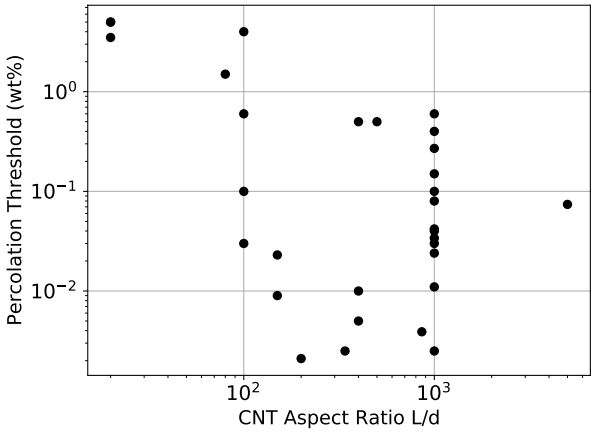

Figure 20: Graph of the percolation threshold of various CNT in epoxy dispersions with changing aspect ratio, data taken from the work of Bauhofer and Kovacs [56]

Fibre surface modification, in the form of deposition and growth of conductive particles, can enhance the conductivity by creating a layer that reduces the particle separation, as shown schematically in figure 21.

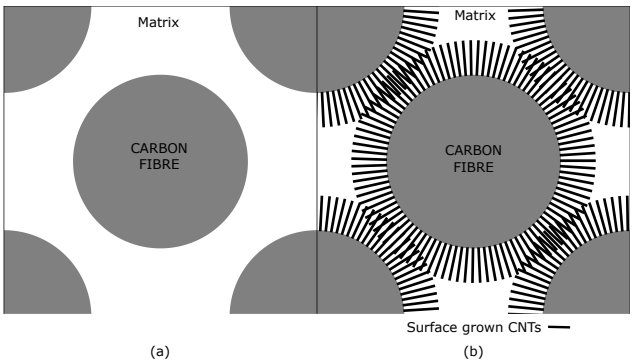

Figure 21: A schematic showing the cross sections of unmodified (a) and modified (b) carbon fibres.

This makes the gaps between the carbon fibres smaller. The

method is limited because conductive additives that are deposited on the fibre surface do not significantly decrease the size of the resin-rich regions between fibres. This explains the improved conductivities of $465\,\%$, $180\,\%$, $138\,\%$ and $2761\,\%$ as shown in table 20.

Interleaving improves the conductivity of CFRPs by different mechanisms depending on the type and form of the material used for the interleave. A dense interleave will improve the overall conductivity by being a highly conductive layer. A dense conductive interleave that does not form an interpenetrative network with the resin will still have resin-rich regions both above and below it. The interpenetration of the matrix into the interleaves is important for the electrical conductivity as well as mechanical properties. As shown schematically in figure 22, the interpenetration of the matrix and the interleave reduces the size of the resin-rich region between the fibre and conductive interleave. Using metal coated polymer fibres veils allows for interpenetration of the interleave, whereas a solid interleave allows no penetration unless it is actively modified by sanding/drilling [9]. An important consideration for interpenetration is the compatibility of the matrix and the bulk interleaving material. Similar materials with high chemical compatibility will have high affinity for each other, and will tend to form interpenetrating networks with higher improvement in properties.

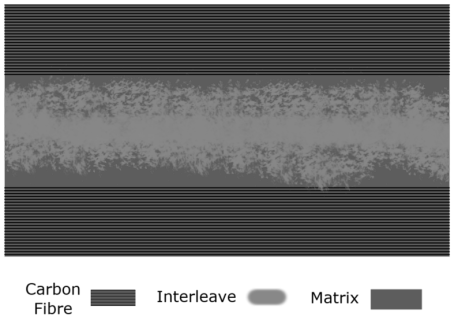

Figure 22: A schematic of an interleaved composite which has formed an inter penetrative network with the electrically conductive interleaving material.

4. Deformation Detection and Structural Health Monitoring

4.1. Deformation

The deformation of both modified resin CFRPs and interleaved CFRPs shows some change in electrical conductivity due to the conductive nature of the carbon fibres themselves. Work done on CNTs reinforced epoxy shows changes in conductivity under deformation [85, 86]. As shown in figures 24a and 24c, bending deformation causes particles on the tensile side to move further apart and particles on the compressive side to move closer together which affects the conductivity. Therefore nanoparticle modified interleaves (such as those made by Li et al. [9]) and nanoparticle modified resin CFRPs show a change in the electrical conductivity when deformed. Figures 24b and 24d show the schematics of the bending of a composite with a fibrous interleave. With a conductive interleave with piezoresistive properties this should change conductivity as the fibres are stretched by the bending. Yang et al. [87] showed the strain sensing capabilities of buckypaper (BP) loaded with graphite nanoplatelets (GnP). The results showed a gauge factor of 10.83 for in-situ strain sensing of the BP when stuck to an epoxy resin surface. The gauge factor is a measure of the change in resistance of the sample with deformation described by equation 4.

$$G = \frac{\Delta R}{R} \tag{4}$$

where G is the gauge factor, ΔR is the change in resistance under deformation, R is the resistance with no deformation. The in-situ results also show good repeatability with little change in the gauge factor after multiple strain cycles.

Datta et al. [50] used buckypaper interleaves within GFRPs as strain sensors. The results show a consistently high sensitivity to strain even after multiple cycles. Although the gauge factor drops during the first few cycles it becomes stable allowing for consistent strain measurement. The buckypaper is responsive to strain mainly due to the change in the CNT contact resistance as it is deformed.

CFRPs constructed with veil interleaves show a change in conductivity as the fibres are put under tension [88]. But other work using silver nanoparticles dispersed in electropsun polymer fibres suggests the change is minimal for strains in the region $0\,\%$ to $5\,\%$ [89–91]. There is no work which concludes that the conductivity of metal coated polymer veils (such as those used by Guo et al. [36] or Barjasteh et al [76]) have conductivity that varies significantly under tension.

Qureshi et al. [92] have shown that silver coated nylon yarns can be used as strain sensors within GFRPs. They coated nylon yarns with silver nano-particles and placed them within the GFRPs during manufacturing. The yarns were each aligned in a specific direction to detect strain in that direction. The results show gauge factors in the range of 21 to 26. Chopped glass fibre composites were used to create isotropic composite with high internal resistance, which allowed for better strain detection. Silver coated nylon used similarly in a CFRP may not produce similar results in terms of gauge factor, as the conductive fibres will give a higher base conductivity. The separation between the silver nanoparticles along the length of the yarns will increase when the yarn is stretched leading to a decrease in conductivity.

Rodríguez-González et al. [93] spray coated glass fibres with MWCNTs to test for flexural loading of the composites. The results showed maximum gauge factors for $0.75\,\mathrm{wt}\%$ composites under three point bend tests. Under three point bend the top surface compresses and the bottom surface is under tension, as such the gauge factor reached $35\,\%$ and $-12\,\%$ for the tensile and compressive sides respectively. These results will allowe for the measurement of the extent of bending in CFRP.

4.2. Structural Health Monitoring

Non-destructive detection and identification of damage in CFRPs has been done using conductivity measurements [39,

40, 49, 83, 94, 95], and eddy current measurements [96–106]. Schueler et al. [40] used multiple probes and created a finite element model of a small composite to detect where and what damage was in the composite. Electrical probes, used to apply current and measure voltages, were attached to the edges of the composites as shown in figure 23. Then a current was applied between sets of two probes with the voltage measured between the other sets of two probes. This allowed for the creation of a finite element (FE) model of the laminates conductivity. When the laminate is damaged the conductivity profile changes. The same system of measurements can be done and compared with the original FE model and therefore any change in the profile shows that the laminate has been damaged. The method works well for a small number of probes, but could be quite slow as the number of current measurements required for a full analysis increases as

$$N_{current} = \frac{P^2 - P}{2} \tag{5}$$

where P is the number of probes, and $N_{current}$ is the number of current measurements. As the accuracy of the position of the damage detected is dependent on the number of probes per metre on each edge. Schueler et al. [40] worked with a set of sixteen probes with four on each edge of the composite. Equation 5 gives 120 different measurements to map the composite. Using $52\,\mathrm{mm}$ by $52\,\mathrm{mm}$ samples cut from a single layer of UD prepreg meant there was one probe every $13\,\mathrm{mm}$. Assuming a similar number of probes per meter for a larger composite of $1\,\mathrm{m}$ by $1\,\mathrm{m}$, it would require 77 probes per meter. To fully map this would require $\approx$6000 different currents to be applied, along with a similar number of voltage measurements for each applied current. This gives a total of over 36×10^6 individual measurements. But for larger composite structures, such as aircraft or cars, the size of the damage that is concerning is larger, so less sensitivity will be needed. Almuhammadi et al. [39] produced

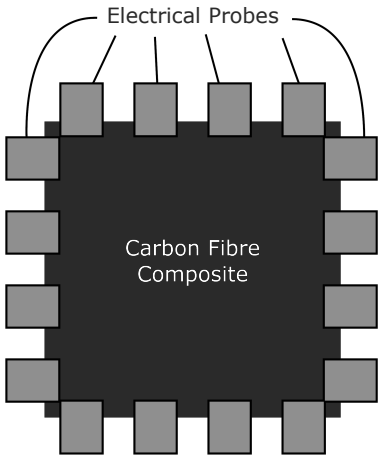

Figure 23: Diagram of carbon fibre laminate (dark grey) with 4 probes attached to each edge (grey). The probes are used to apply current and measure voltage. As in the work of schueler et al. [40]

a more real-time damage and deformation detection method, but this only measured surface damage and deformation. Tallman et al. [95] modelled non-destructive damage detection on CNT based resin CFRPs similar to the work of Schueler et al. [40] where probes were mounted on the edge. They looked at the effect of the alignment of CNTs and the CNT content on the sensitivity of the damage detection. Their modelling results agreed well with experimental data and showed that the damage detection was improved for low CNT contents ($1\,\mathrm{wt}\%$) but became less sensitive as the content increased. Figure 25

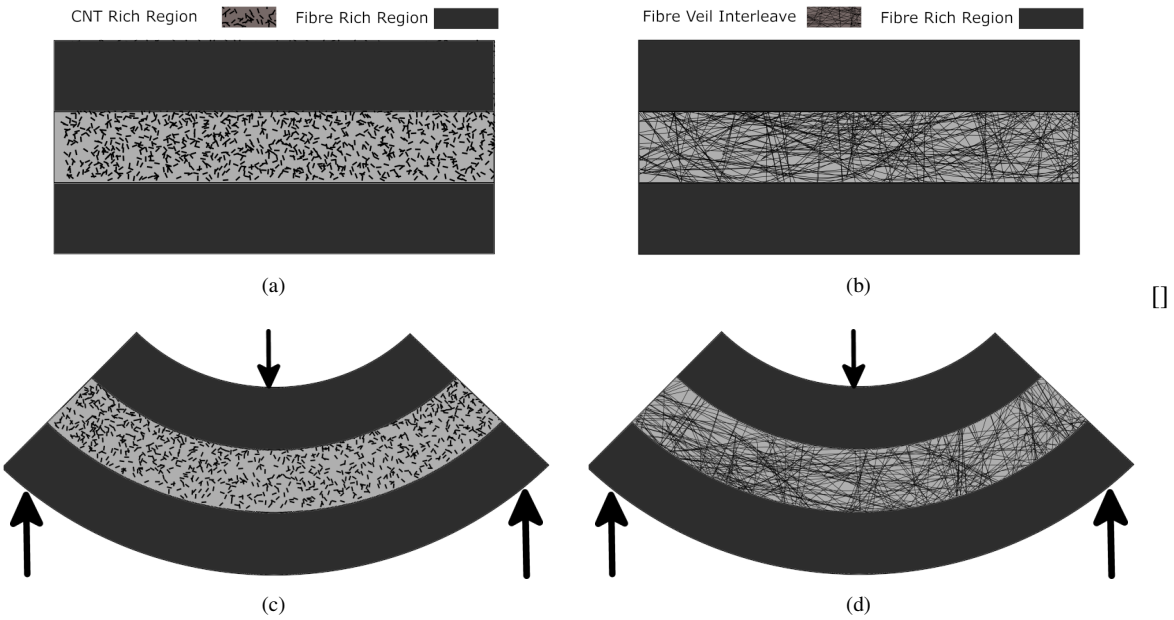

[]

Figure 24: Schematic of exaggerated three-point-bend of composites with dispersed particles (a and c) and fibre interleaves (b and d), showing the increase in particle separation and the stretching of the fibres.

shows schematically how fractures can decrease the conductivity by breaking conductive paths. The sensitivity of this method decreases at high concentrations as there are many percolating paths, meaning more have to be broken to produce a significant change in the resistance.

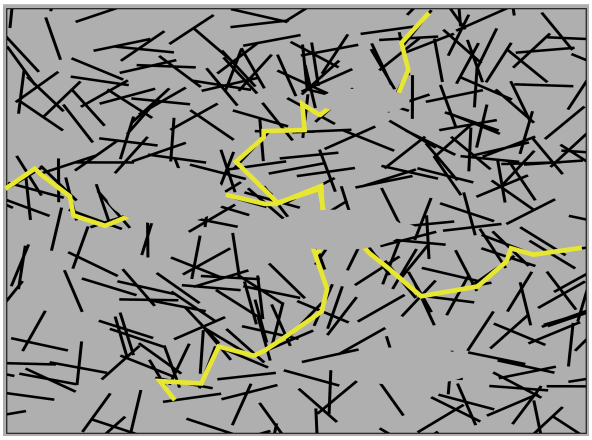

Figure 25: A schematic showing how crack damage in a CNT network breaks the percolation, this will reduce the conductivity.

Todoroki et al. [83] used resistance measurements to detect delamination in composites. Using repeat resistance measurements and a neural network they were able to locate the delamination damage within the composite. The setup used to detect the damage consisted of electrodes placed only on one surface similar to any system that would be used in aerospace damage detection. Surface grafting, deposition, and growth can improve fibre/matrix delamination detection, as when the fibre and matrix separate this increases the distance between fibres reducing the conductivity. Figure 26 shows that the formation of cracks between fibres or fibre/matrix delamination will increase the resistance between adjacent fibres. The delamination of conductive interleaves in the interlaminar region can be easily detected as the separation of the conductive interleave from the resin increases the resistance of the CFRP.

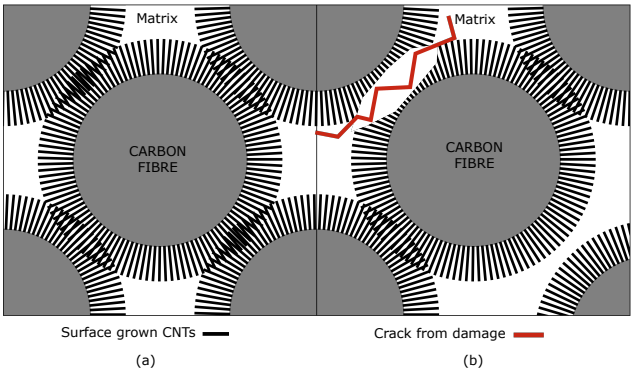

Figure 26: A schematic of pristine carbon fibres in matrix with surface grown carbon nanotubes (a), diagram of damaged surface nanotubes due to delamination or crack between the carbon fibre (b).

5. Discussion

From the work reviewed it is clear that there are many different possible routes to consider when attempting to improve through-thickness electrical conductivity in CFRPs. The conductivity improvement depends on the conductive material used and the method. Table 20 shows that the conductivity of unmodified CFRPs varies quite dramatically, as such the success of the conductivity improvement of a technique is considered based on the percentage increase in the through-thickness conductivity. However it is important to consider final electrical conductivity value of samples, as this is important for the final application of the composite.

Table 20 shows that the use of CNTs as a resin additive produces very large percentage increases of up to $10\,000\,\%$, with the use of other additives showing smaller improvements $83\,\%$ to $2900\,\%$. The coating of fibres produces mostly lower percentage increases ($138\,\%$ to $2790\,\%$) when compared with other methods using the same conductive materials, suggesting fibre surface modification is not very effective. The use of a polymeric interleave produces a negative result due to the insulating nature of the interleaving material. The effect of the insulation of the interleave is reduced by coating it with a conductive material, such as metal, or conductive nanoparticles (GNP, CNT). Interleaves are limited in their effectiveness as they only act where they are placed between the carbon fibre layers. Stitching shows the largest percentage increase in through-thickness electrical conductivity ($12\,440\,\%$), because the stitching used vertical stitching of highly conductive silver coated nylon yarns. 3D stitching of fibres can be a complex process and the introduction of vertical fibres can create resin pockets which negatively affect mechanical properties.

The work reviewed suggests that the mechanical properties of the composites can be retained by avoiding easy damage propagation routes such as delamination along interleave surfaces, voids caused by high viscosity, or delamination at the fibre/matrix interface due to reduced wetting. Any future work will need to use materials and processing techniques that reduce the chance of defects. The work of both Guo et al. [73] and Li et al. [9] have shown considerable simultaneous improvement in interlaminar fracture toughness and through-thickness electrical conductivity. With both pieces of work taking advantage of tough thermoplastics to improve the interlaminar properties whilst incorporating conductive additives to improve conductivity. An important distinction in their work is the form of the interleave. The veils used by Guo et al. [73] show a much greater improvement in mechanical properties than the moulded sheets of Li et al. [9] despite both using PA12 nylon. As shown by Guo et al. [36, 73] the interaction of the interleave and matrix contributes greatly to the interlaminar fracture toughness properties of the final CFRP. Strong interfacial bonding is required when using an interleave, a weak interaction can greatly reduce the interlaminar toughness [26]. The resin needs to penetrate into the interleave to create mechanical bonding, which increases the strength and the surface area of contact. This is also supported by the improvement in the interlaminar fracture toughness of plasma-treated PA12 CTF interleaved CFRPs

compared to untreated PA12 interleaved CFRPs. The plasma treatment changes the PA12 surface increasing the topology as well as producing more functional groups that can bond with the resin during curing [9].

Bian et al. [107] work looks at the interpenetration of thermoplastics and epoxy resin by choosing a thermoplastic with a good compatibility with the resin as well as adding $5\,\mathrm{wt}\%$ polystyrene to the epoxy to reduce the curing rate. The reduction in the curing rate allows for the formation of a semi-interpenetrated networks between the epoxy and compatible thermoplastic. Curing at a temperature of $120\,^{\circ}\mathrm{C}$ also showed improvement over curing at $80\,^{\circ}\mathrm{C}$, which was attributed to lower viscosity of the polymers [107]. The resulting composites show improved delamination resistance with increasing depth of the semi-IPNs (semi-interpenetrated networks). Thus the chemical compatibility between the interleaving thermoplastic and the matrix resin plays a major role in enhancing the interlaminar fracture toughness of the CFRP.

6. Conclusions

Multiple methods for modifying the through-thickness electrical conductivity have been discussed in this review. Reasons for the successes and failures of the methods are reported in order to understand which methods should be focused upon. The effect of the different electrical conductivity modifying techniques on the mechanical properties is considered with the methods for the mitigation of weakening effects. The mechanisms for the improvement of the conductivity by different techniques is presented with discussion of how the modifications could be used to improve in-situ damage and deformation detection. The work discussed shows that it is possible to improve through-thickness electrical conductivity whilst simultaneously improving mechanical properties of CFRPs. The addition of conductive materials to CFRPs can improve in-situ damage and deformation detection by resistance measurements and make the composite multifunctional.

Table 20: Summary of different enhancement techniques used and their effects on the through-thickness electrical conductivity and the mechanical properties of the resultant CFRPs. ND is written if no data for mechanical properties was given. The table is split into the previously discussed main categories of resin modification, fibre surface modification, interleaving, and other methods

Fibre and Resin	Fibre volume Percentage	Conductive Materials	Processing Technique	Original Conductivity σ_{0z} (S m^{-1})	Max Improved Conductivity σ_z (S m^{-1})	Max Percentage Change in σ_z	Changes in Mechanical Properties
Resin Modification							
Carbon Fibre Fabric Epoxy	60	PANI/DVB with GO or MWCNT	Nanoparticle sonication dispertion with single step cure and doping of PANI	6.04×10^{-2} (CF/Epoxy)	22.4	+37 000	ND [108]
Carbon fabric DVB	ND	GO with PANI	GO dispersed in PANI	6.17×10^{-5}	6.36×10^{-2}	+10 300	ND [109]
T700SC 12K Bismaleide	57	CNT	Sonication and shear mixing	0.16	16.4	+10 000	Improved compression and ILSS [55]
Toray T700 RTM6 Epoxy	67	DWCNT	Sonication Dispersion	0.0066	0.53	+7930	ND [21]
T700 Fibre with Epoxy Resin	ND	GnP	Three Roll Mill	≈0.02	0.60	+2900	Small improvement in ILSS and flexural modulus [62]
Plain Woven TR3110M fibre Epoxy	ND	PANI/DBSA/ PTSA/DVB	Single step doping and curing	2.7	74	+2640	Significantly reduced flexural strength [64]
Plain weave carbon fibres Bisphenol-A epoxy resin		MWCNT and CNF	Dispersed and aligned in the z-direction	2.3 ± 0.2	21 ± 4	+910	Improved flexural strength and tensile strength [110].
Plain Weave Bisphenol-F epoxy	45	GNP AgNW AgNP	Sonication Dispersion	0.077	0.3	+290	Significant decrease in compressive and tensile strength with AgNW. Generally no significant change [63].
UD Fabric Naxxores ER 5300	57	GO	Planetary mixing	5.43	18	+230	Increased ILSS with GO content up to 0.63 vol% [24].
T300J Toray UD Bisphenol A Epoxy	65.9	CB and CuCl	Planetary ball mill	30.3	55.6	+83	Improvement Mode I type interlaminar fracture toughness, no change in Mode II type [25].
Epoxy resin UD carbon fibre fabric	ND	MWCNT with surface buckypaper layer	MWCNT dispersed in resin	4 ± 1	5.3 ± 0.4	+32	Small decrease in ILSS, not significant [111].
Woven Fabric DVB resin	ND	PANI-DBSA/DVB	Semi-doping of PANI followed by curing	ND	135	N/A	Reduced flexural strength compared with CF/Epoxy minimal for highest conductivity [68].
SGL Twill Bisphenol-F Epoxy	ND	SWNCNT	Sonication Dispersion	ND	66	N/A	Compression improved with degassing little change in flexural and tensile strengths [20].
Fibre surface modification							
12k with epoxy resin	ND	CNT	Grown on carbon fibre surface by Chemical Vapor Deposition	3×10^{-3}	3.8×10^{-1}	+12 600	ND [112].
UD PaN Fabric	55.9	CNT	Electrophoretic Deposition	0.0065	0.186	+2761	Improved ILSS, maximum for two step deposition process [72].
Plain weave carbon fibre fabric Biphenol A resin	ND	GNP	Low temperature carbon growth on fibre surface with GNP dispersed in epoxy resin.	5 ± 1	84 ± 9	+1680	Improved flexural strength and ILSS [16].
2/2 Twill DGEBA	50	CNT	PTCVD	0.15	0.7	+465	Single fibres showed improved tensile strength [22].

PAN 12K UD Epon 828	ND	GNP	Continuous Coating	2.5	7	+180	Improved ILSS [47].
UD HCU302 Bisphenol A epoxy	ND	GO	Electrophoresis	13	31	+138	Improved ILSS and Mode I interlaminar fracture toughness, maximum for non-reduced graphene oxide coated fibres [48].
Interleaving							
UD Epoxy Prepreg	54	MWCNT dispersed in thermoplastic	Layered between prepreg	2×10^{-5}	2×10^{-3}	+8822	Decreased ILSS [113].
T700SC 12K Bismaleide	57	Chopped fibre resin layers	Interleaved with different resin contents/thicknesses	0.43	18	+4080	No significant change in compressive strength and ILSS [77].
UD Toray T801 Epoxy Prepreg	53.4	Silver Plated PA and kevlar veils	Interleaved	12.2	300	+2360	Improved Mode I and Mode II interlaminar fracture toughness, best improvement with nylon interleave [73].
UD Prepreg Epoxy T700	63	PA12 with CNTs	Interleaved and Plasma treated	0.0086	0.18	+1990	Mode I and Mode II fracture toughness were weakened with the interleave, but improved with the plasma treated interleave [9]
UD 12K epoxy resin prepreg	56.85	CNT doped non woven copolyamide veils	Interleaved between prepreg layers	0.690 ± 0.082	3.16 ± 0.40	+457	greatly reduced ILSS due to lower FVF [114]
T300-3K plain woven fabric	48	Buckypaper	Interleave and Top Layer	≈10	52	+420	Decrease in flexural strength and modulus [4]
UD Fibre Epoxy resin	54.7	Paper and AgNW	Interleaved Between prepregs	4.7	17.9	+280	Significant decreased in both the Mode I and Mode II interlaminar fracture toughness [36].
UD Toray T800 Epoxy Resin Prepreg	52.4	AgNW coated PEK-C	Interleaved between dry fibre	12.2	1.5	−87	Increases in both Mode I and Mode II interlaminar fracture toughness [26].
Ud T300 Toray Loctite BZ 9100 Aero	54	PA12 with Graphene	Interleave graphene coated PA12	ND	0.0025	N/A	Considerable Improvement in both G_I and G_{II} toughness [76].
Other Methods							
T700 UD Epoxy Prepreg	ND	Carbon, Steel, Titatium, Copper	Z-Pinning	0.2	9.05×10^5	$+1.1 \times 10^8$	ND [115]
UD prepreg	59.4	Silver coated knitting yarns	Stitching between fibres	5.0	627.0	+12 440	ND [8]
T700 UD carbon fibre epoxy prepreg	ND	$MWCNT - NH_2$, $MWCNT - BGE$	Spray coating of prepreg	72 ± 3	300 ± 4	317	Slight improvement in ILSS, though not significant [116]

Acknowledgements

The authors acknowledge the support from EPSRC Centre for Doctoral Training in Soft Matter and Functional Interfaces (EP/Lo15536/1).

References

[1] N.H.Nash, T.M.Young, P.T.McGrail, W.F.Stanley, Inclusion of a thermoplastic phase to improve impact and post-impact performances of carbon fibre reinforced thermosetting composites – a review, Materials and Design 85 (2015) 582–597. doi:10.1016/j.matdes.2015.07.001.

[2] V. Kostopoulos, A. Baltopoulos, P. Karapappas, A. Vavouliotis, A. Paipetis, Impact and after-impact properties of carbon fibre reinforced composites enhanced with multi-wall carbon nanotubes, Composites Science and Technology 70 (4) (2010) 553–563. doi:10.1016/j.compscitech.2009.11.023.

[3] V. Kumar, Y. Zhou, G. Shambharkar, V. Kunc, T. Yokozeki, Reduced de-doping and enhanced electrical conductivity of polyaniline filled phenol-divinylbenzene composite for potential lightning strike protection application, Synthetic Metals 249 (2019) 81–89. doi:10.1016/j.synthmet.2019.02.003.

[4] V. Kumar, S. Sharma, A. Pathak, B. P. Singh, S. R. Dhakate, T. Yokozeki, T. Okada, T. Ogasawara, Interleaved MWCNT buckypaper between CFRP laminates to improve through-thickness electrical conductivity and reducing lightning strike damage, Composite Structures 210 (2019) 581–589. doi:10.1016/j.compstruct.2018.11.088.

[5] H. Chu, Q. Xia, Z. Zhang, Y. Liu, J. Leng, Sesame-cookie topography silver nanoparticles modified carbon nanotube paper for enhancing lightning strike protection, Carbon 143 (2019) 204–214. doi:10.1016/j.carbon.2018.11.022.

[6] J. hua Han, H. Zhang, M. ji Chen, D. Wang, Q. Liu, Q. lei Wu, Z. Zhang, The combination of carbon nanotube buckypaper and insulating adhesive for lightning strike protection of the carbon fiber/epoxy laminates, Carbon 94 (2015) 101–113. doi:10.1016/j.carbon.2015.06.026.

[7] V. Kumar, T. Yokozeki, T. Okada, Y. Hirano, T. Goto, T. Takahashi, A. A. Hassen, T. Ogasawara, Polyaniline-based all-polymeric adhesive layer: An effective lightning strike protection technology for high residual mechanical strength of CFRPs, Composites Science and Technology 172 (2019) 49–57. doi:10.1016/j.compscitech.2019.01.006.

[8] J. Rehbein, P. Wierach, T. Gries, M. Wiedemann, Improved electrical conductivity of NCF-reinforced CFRP for higher damage resistance to lightning strike, Composites Part A: Applied Science and Manufacturing 100 (2017) 352–360. doi:10.1016/j.compositesa.2017.05.014.

[9] W. Li, D. Xiang, L. Wang, E. Harkin-Jones, C. Zhao, B. Wang, Y. Li, Simultaneous enhancement of electrical conductivity and interlaminar fracture toughness of carbon fiber/epoxy composites using plasma-treated conductive thermoplastic film interleaves, RSC Advances 8 (47) (2018) 26910–26921. doi:10.1039/c8ra05366a.

[10] J. Chen, Z. Fu, Y. Zhao, Resistance behaviour of carbon fibre-reinforced polymers subjected to lightning strikes: Experimental investigation and application, Advanced Composites Letters 28 (2019) 2633366X19892272. arXiv:https://doi.org/10.1177/2633366X19892272, doi:10.1177/2633366X19892272.

[11] F. Wang, Y. Zhang, X. Ma, Z. Wei, J. Gao, Lightning ablation suppression of aircraft carbon/epoxy composite laminates by metal mesh, Journal of Materials Science & Technology 35 (11) (2019) 2693 – 2704. doi:https://doi.org/10.1016/j.jmst.2019.07.010.

[12] V. Bedel, A. Lonjon, E. Dantras, M. Bouquet, Innovative conductive polymer composite coating for aircrafts lightning strike protection, Journal of Applied Polymer Science 137 (20) (2020) 48700. arXiv:https://onlinelibrary.wiley.com/doi/pdf/10.1002/app.48700, doi:10.1002/app.48700.

[13] Q. Xia, H. Mei, Z. Zhang, Y. Liu, Y. Liu, J. Leng, Fabrication of the silver modified carbon nanotube film/carbon fiber reinforced polymer composite for the lightning strike protection application, Composites Part B: Engineering 180 (2020) 107563. doi:https://doi.org/10.1016/j.compositesb.2019.107563.

[14] J. Sun, X. Yao, W. Xu, J. Chen, Y. Wu, Evaluation method for lightning damage of carbon fiber reinforced polymers subjected to multiple lightning strikes with different combinations of current components, Journal of Composite Materials 54 (1) (2020) 111–125. arXiv:https://doi.org/10.1177/0021998319860562, doi:10.1177/0021998319860562.

[15] K. Ueno, N. Miki, Y. Baba, N. Nagaoka, H. Tsubata, T. Nishi, Electromagnetic and thermal analysis of a multilayer cfrp panel struck by lightning with the fdtd method, IEEJ Transactions on Electrical and Electronic Engineering 15 (1) (2020) 157–158. arXiv:https://onlinelibrary.wiley.com/doi/pdf/10.1002/tee.23038, doi:10.1002/tee.23038.

[16] A. Duongthipthewa, Y. Su, L. Zhou, Electrical conductivity and mechanical property improvement by low-temperature carbon nanotube growth on carbon fiber fabric with nanofiller incorporation, Composites Part B: Engineering 182 (2020) 107581. doi:https://doi.org/10.1016/j.compositesb.2019.107581.

[17] T. Harrell, O. Thomsen, J. Dulieu-Barton, S. Madsen, Damage in cfrp composites subjected to simulated lighting strikes - assessment of thermal and mechanical responses, Composites Part B: Engineering 176 (2019) 107298. doi:https://doi.org/10.1016/j.compositesb.2019.107298.

[18] S. Kamiyama, Y. Hirano, T. Okada, K. Sawaki, T. Sonehara, T. Ogasawara, Damage behavior of cfrp subjected to simulated lightning current under air, reduced-pressure air, and n2 environments, Composite Structures 230 (2019) 111519. doi:https://doi.org/10.1016/j.compstruct.2019.111519.

[19] G. Wan, Q. Dong, J. Zhi, Y. Guo, X. Yi, Y. Jia, Analysis on electrical and thermal conduction of carbon fiber composites under lightning based on electrical-thermal-chemical coupling and arc heating models, Composite Structures 229 (2019) 111486. doi:https://doi.org/10.1016/j.compstruct.2019.111486.

[20] M. Burkov, A. Eremin, Hybrid cfrp/swcnt composites with enhanced electrical conductivity and mechanical properties, Journal of Materials Engineering and Performance 27 (11) (2018) 5984–5991. doi:10.1007/s11665-018-3695-x.

[21] I. E. Sawi, P. A. Olivier, P. Demont, H. Bougherara, Processing and electrical characterization of a unidirectional CFRP composite filled with double walled carbon nanotubes, Composites Science and Technology 73 (2012) 19–26. doi:10.1016/j.compscitech.2012.08.016.

[22] T. Pozegic, I. Hamerton, J. Anguita, W. Tang, P. Ballocchi, P. Jenkins, S. Silva, Low temperature growth of carbon nanotubes on carbon fibre to create a highly networked fuzzy fibre reinforced composite with superior electrical conductivity, Carbon 74 (2014) 319–328. doi:10.1016/j.carbon.2014.03.038.

[23] B. A. Newcomb, H. G. Chae, The properties of carbon fibers, in: Handbook of Properties of Textile and Technical Fibres, Elsevier, 2018, pp. 841–871. doi:10.1016/b978-0-08-101272-7.00021-3.

[24] E. C. Senis, I. O. Golosnoy, J. M. Dulieu-Barton, O. T. Thomsen, Enhancement of the electrical and thermal properties of unidirectional carbon fibre/epoxy laminates through the addition of graphene oxide, Journal of Materials Science 54 (12) (2019) 8955–8970. doi:10.1007/s10853-019-03522-8.

[25] D. Zhang, L. Ye, S. Deng, J. Zhang, Y. Tang, Y. Chen, CF/EP composite laminates with carbon black and copper chloride for improved electrical conductivity and interlaminar fracture toughness, Composites Science and Technology 72 (3) (2012) 412–420. doi:10.1016/j.compscitech.2011.12.002.

[26] M. Guo, X. Yi, G. Liu, L. Liu, Simultaneously increasing the electrical conductivity and fracture toughness of carbon–fiber composites by using silver nanowires-loaded interleaves, Composites Science and Technology 97 (2014) 27–33. doi:10.1016/j.compscitech.2014.03.020.

[27] X. Ma, F. Wang, Z. Wei, D. Wang, B. Xu, Transient response predication of nickel coated carbon fiber composite subjected to high altitude electromagnetic pulse, Composite Structures 226 (2019) 111307. doi:https://doi.org/10.1016/j.compstruct.2019.111307.

[28] V. P. Shaw, K. Jagatheesan, A. Ramasamy, Mechanical and electromagnetic shielding behaviours of thermoplastic conductive composite: influence of yarn structure and process variables, The Journal of The Textile Institute 0 (0) (2019) 1–8. arXiv:https://doi.org/10.1080/00405000.2019.1688903, doi:10.1080/00405000.2019.1688903.

[29] L. Vovchenko, O. Lozitsky, L. Matzui, V. Oliynyk, V. Zagorodnii, M. Skoryk, Electromagnetic shielding properties of epoxy composites with hybrid filler nanocarbon/batio3, Materials Chemistry and Physics 240 (2020) 122234. doi:https://doi.org/10.1016/j.matchemphys.2019.122234.

[30] I. C. Kim, K. H. Kwon, W. N. Kim, Effects of hybrid fillers on the electrical conductivity, emi shielding effectiveness, and flame retardancy of pbt and polyasa composites with carbon fiber and mwcnt, Journal of Applied Polymer Science 136 (44) (2019) 48162. arXiv:https://onlinelibrary.wiley.com/doi/pdf/10.1002/app.48162, doi:10.1002/app.48162.

[31] A. Katunin, K. Krukiewicz, R. Turczyn, P. Sul, K. Dragan, Lightning strike resistance of an electrically conductive CFRP with a CSA-doped PANI/epoxy matrix, Composite Structures 181 (2017) 203–213. doi:10.1016/j.compstruct.2017.08.091.

[32] P. Rajesh, F. Sirois, D. Therriault, Damage response of composites coated with conducting materials subjected to emulated lightning strikes, Materials & Design 139 (2018) 45–55. doi:10.1016/j.matdes.2017.10.017.

[33] V. Kumar, T. Yokozeki, T. Okada, Y. Hirano, T. Goto, T. Takahashi, T. Ogasawara, Effect of through-thickness electrical conductivity of CFRPs on lightning strike damages, Composites Part A: Applied Science and Manufacturing 114 (2018) 429–438. doi:10.1016/j.compositesa.2018.09.007.

[34] M. Gagné, D. Therriault, Lightning strike protection of composites, Progress in Aerospace Sciences 64 (2014) 1–16. doi:10.1016/j.paerosci.2013.07.002.

[35] H. Che, M. Gagné, P. S. M. Rajesh, J. E. Klemberg-Sapieha, F. Sirois, D. Therriault, S. Yue, Metallization of carbon fiber reinforced polymers for lightning strike protection, Journal of Materials Engineering and Performance 27 (10) (2018) 5205–5211. doi:10.1007/s11665-018-3609-y.

[36] M. Guo, X. Yi, Effect of paper or silver nanowires-loaded paper interleaves on the electrical conductivity and interlaminar fracture toughness of composites, Aerospace 5 (3) (2018) 77. doi:10.3390/aerospace5030077.

[37] H. Kim, Enhanced crack detection sensitivity of carbon fiber composites by carbon nanotubes directly grown on carbon fibers, Composites Part B: Engineering 60 (2014) 284–291. doi:10.1016/j.compositesb.2013.12.063.

[38] J. Zhang, X. Zhang, X. Cheng, Y. Hei, L. Xing, Z. Li, Lightning strike damage on the composite laminates with carbon nanotube films: Protection effect and damage mechanism, Composites Part B: Engineering 168 (2019) 342–352. doi:10.1016/j.compositesb.2019.03.054.

[39] K. Almuhammadi, A. Yudhanto, G. Lubineau, Real-time electrical impedance monitoring of carbon fiber-reinforced polymer laminates undergoing quasi-static indentation, Composite Structures 207 (2019) 255–263. doi:10.1016/j.compstruct.2018.09.030.

[40] R. Schueler, S. P. Joshi, K. Schulte, Damage detection in CFRP by electrical conductivity mapping, Composites Science and Technology 61 (6) (2001) 921–930. doi:10.1016/s0266-3538(00)00178-0.

[41] S. Wang, D. Chung, Self-sensing of flexural strain and damage in carbon fiber polymer-matrix composite by electrical resistance measurement, Carbon 44 (13) (2006) 2739 – 2751. doi:https://doi.org/10.1016/j.carbon.2006.03.034.

[42] D.-C. Seo, J.-J. Lee, Damage detection of cfrp laminates using electrical resistance measurement and neural network, Composite Structures 47 (1) (1999) 525 – 530, tenth International Conference on Composite Structures. doi:https://doi.org/10.1016/S0263-8223(00)00016-7.

[43] H. Zhang, E. Bilotti, T. Peijs, The use of carbon nanotubes for damage sensing and structural health monitoring in laminated composites: a review, Nanocomposites 1 (4) (2015) 167–184. doi:10.1080/20550324.2015.1113639.

[44] M. Monti, M. Natali, J. M. Kenny, L. Torre, A. D'Amore, D. Acierno, L. Grassia, MWNT-doped epoxy matrix for detecting impact damages in fiber reinforced composites by electrical resistance measurements, AIP, 2010. doi:10.1063/1.3455631.

[45] A. Baltopoulos, N. Polydorides, L. Pambaguian, A. Vavouliotis, V. Kostopoulos, Exploiting carbon nanotube networks for damage assessment of fiber reinforced composites, Composites Part B: Engineering 76 (2015) 149–158. doi:10.1016/j.compositesb.2015.02.022.

[46] C. Li, T.-W. Chou, Modeling of damage sensing in fiber composites using carbon nanotube networks, Composites Science and Technology 68 (15-16) (2008) 3373–3379. doi:10.1016/j.compscitech.2008.09.025.

[47] W. Qin, F. Vautard, L. T. Drzal, J. Yu, Mechanical and electrical properties of carbon fiber composites with incorporation of graphene nanoplatelets at the fiber–matrix interphase, Composites Part B: Engineering 69 (2015) 335–341. doi:10.1016/j.compositesb.2014.10.014.

[48] L. Bhanuprakash, S. Parasuram, S. Varghese, Experimental investigation on graphene oxides coated carbon fibre/epoxy hybrid composites: Mechanical and electrical properties, Compos. Sci. Technol. 179 (2019) 134–144. doi:https://doi.org/10.1016/j.compscitech.2019.04.034.

[49] J. Cagáň, J. Pelant, M. Kyncl, M. Kadlec, L. Michalcová, Damage detection in carbon fiber–reinforced polymer composite via electrical resistance tomography with gaussian anisotropic regularization, Structural Health Monitoring 18 (5-6) (2019) 1698–1710. arXiv:https://doi.org/10.1177/1475921718820013, doi:10.1177/1475921718820013.

[50] S. Datta, R. K. Neerukatti, A. Chattopadhyay, Buckypaper embedded self-sensing composite for real-time fatigue damage diagnosis and prognosis, Carbon 139 (2018) 353–360. doi:10.1016/j.carbon.2018.06.059.

[51] D.-J. Kwon, P.-S. Shin, J.-H. Kim, Z.-J. Wang, K. L. DeVries, J.-M. Park, Detection of damage in cylindrical parts of carbon fiber/epoxy composites using electrical resistance (ER) measurements, Composites Part B: Engineering 99 (2016) 528–532. doi:10.1016/j.compositesb.2016.06.050.

[52] V. Dikshit, S. Bhudolia, S. Joshi, Multiscale polymer composites: A review of the interlaminar fracture toughness improvement, Fibers 5 (4) (2017) 38. doi:10.3390/fib5040038.

[53] Z. Spitalsky, D. Tasis, K. Papagelis, C. Galiotis, Carbon nanotube–polymer composites: Chemistry, processing, mechanical and electrical properties, Progress in Polymer Science 35 (3) (2010) 357–401. doi:10.1016/j.progpolymsci.2009.09.003.

[54] J. Sandler, M. Shaffer, T. Prasse, W. Bauhofer, K. Schulte, A. Windle, Development of a dispersion process for carbon nanotubes in an epoxy matrix and the resulting electrical properties, Polymer 40 (21) (1999) 5967–5971. doi:10.1016/s0032-3861(99)00166-4.

[55] Z. Zhao, B. Zhang, Y. Du, Y. Hei, X. Yi, F. Shi, G. Xian, MWCNT modified structure-conductive composite and its electromagnetic shielding behavior, Composites Part B: Engineering 130 (2017) 21–27. doi:10.1016/j.compositesb.2017.07.033.

[56] W. Bauhofer, J. Z. Kovacs, A review and analysis of electrical percolation in carbon nanotube polymer composites, Composites Science and Technology 69 (10) (2009) 1486–1498. doi:10.1016/j.compscitech.2008.06.018.

[57] T. Yokozeki, Y. Iwahori, S. Ishiwata, K. Enomoto, Mechanical properties of CFRP laminates manufactured from unidirectional prepregs using CSCNT-dispersed epoxy, Composites Part A: Applied Science and Manufacturing 38 (10) (2007) 2121–2130. doi:10.1016/j.compositesa.2007.07.002.

[58] T. W. Ebbesen, H. J. Lezec, H. Hiura, J. W. Bennett, H. F. Ghaemi, T. Thio, Electrical conductivity of individual carbon nanotubes, Nature 382 (6586) (1996) 54–56. doi:10.1038/382054a0.

[59] W. S. Bao, S. A. Meguid, Z. H. Zhu, G. J. Weng, Tunneling resistance and its effect on the electrical conductivity of carbon nanotube nanocomposites, Journal of Applied Physics 111 (9) (2012) 093726. doi:10.1063/1.4716010.

[60] H. Ridaoui, A. Jada, L. Vidal, J.-B. Donnet, Effect of cationic surfactant and block copolymer on carbon black particle surface charge and size, Colloids and Surfaces A: Physicochemical and Engineering Aspects 278 (1-3) (2006) 149–159. doi:10.1016/j.colsurfa.2005.12.013.

[61] L. Belloni, Colloidal interactions, Journal of Physics: Condensed Matter 12 (46) (2000) R549–R587. doi:10.1088/0953-8984/12/46/201.

[62] Y. Li, H. Zhang, Z. Huang, E. Bilotti, T. Peijs, Graphite nanoplatelet modified epoxy resin for carbon fibre reinforced plastics with enhanced properties, Journal of Nanomaterials 2017 (2017) 1–10. doi:10.1155/2017/5194872.

[63] E. Kandare, A. A. Khatibi, S. Yoo, R. Wang, J. Ma, P. Olivier, N. Gleizes, C. H. Wang, Improving the through-thickness thermal and electrical conductivity of carbon fibre/epoxy laminates by exploiting synergy between graphene and silver nano-inclusions, Composites Part A: Applied Science and Manufacturing 69 (2015) 72–82. doi:10.1016/j.compositesa.2014.10.024.

[64] Y. Hirano, T. Yokozeki, Y. Ishida, T. Goto, T. Takahashi, D. Qian, S. Ito, T. Ogasawara, M. Ishibashi, Lightning damage suppression in a carbon fiber-reinforced polymer with a polyaniline-based conductive thermoset matrix, Composites Science and Technology 127 (2016) 1–7. doi:10.1016/j.compscitech.2016.02.022.

[65] T. Nezakati, A. Seifalian, A. Tan, A. M. Seifalian, Conductive polymers: Opportunities and challenges in biomedical applications, Chemical Reviews 118 (14) (2018) 6766–6843. doi:10.1021/acs.chemrev.6b00275.

[66] S. Bhandari, Polyaniline, in: Polyaniline Blends, Composites, and Nanocomposites, Elsevier, 2018, pp. 23–60. doi:10.1016/b978-0-12-809551-5.00002-3.

[67] V. Kumar, T. Yokozeki, T. Goto, T. Takahashi, Mechanical and electrical properties of PANI-based conductive thermosetting composites, Journal of Reinforced Plastics and Composites 34 (16) (2015) 1298–1305. doi:10.1177/0731684415588551.

[68] V. Kumar, T. Yokozeki, T. Goto, T. Takahashi, S. R. Dhakate, B. P. Singh, Irreversible tunability of through-thickness electrical conductivity of polyaniline-based CFRP by de-doping, Composites Science and Technology 152 (2017) 20–26. doi:10.1016/j.compscitech.2017.09.005.

[69] P. K. Gangineni, S. Yandrapu, S. K. Ghosh, A. Anand, R. K. Prusty, B. C. Ray, Mechanical behavior of graphene decorated carbon fiber reinforced polymer composites: An assessment of the influence of functional groups, Composites Part A: Applied Science and Manufacturing 122 (2019) 36–44. doi:10.1016/j.compositesa.2019.04.017.

[70] M. Delamar, G. Désarmot, O. Fagebaume, R. Hitmi, J. Pinsonc, J.-M. Savéant, Modification of carbon fiber surfaces by electrochemical reduction of aryl diazonium salts: Application to carbon epoxy composites, Carbon 35 (6) (1997) 801–807. doi:10.1016/s0008-6223(97)00010-9.

[71] H. S. Bedi, S. S. Padhee, P. K. Agnihotri, Effect of carbon nanotube grafting on the wettability and average mechanical properties of carbon fiber/polymer multiscale composites, Polymer Composites 39 (S2) (2018) E1184–E1195. doi:10.1002/pc.24714.

[72] F. Yan, L. Liu, M. Li, M. Zhang, L. Shang, L. Xiao, Y. Ao, One-step electrodeposition of cu/CNT/CF multiscale reinforcement with substantially improved thermal/electrical conductivity and interfacial properties of epoxy composites, Composites Part A: Applied Science and Manufacturing 125 (2019) 105530. doi:10.1016/j.compositesa.2019.105530.

[73] M. Guo, X. Yi, C. Rudd, X. Liu, Preparation of highly electrically conductive carbon-fiber composites with high interlaminar fracture toughness by using silver-plated interleaves, Composites Science and Technology 176 (2019) 29–36. doi:10.1016/j.compscitech.2019.03.014.

[74] M. Guo, X. Yi, The production of tough, electrically conductive carbon fiber composite laminates for use in airframes, Carbon 58 (2013) 241–244. doi:10.1016/j.carbon.2013.02.052.

[75] W. Li, Y. Li, D. Xiang, C. Zhao, B. Wang, H. Li, H. Han, Simultaneous enhancement of electrical conductivity and interlaminar shear strength of cf/ep composites through mwcnts doped thermoplastic polyurethane film interleaves, Journal of Applied Polymer Science 136 (39) (2019) 47988. arXiv:https://onlinelibrary.wiley.com/doi/pdf/10.1002/app.47988, doi:10.1002/app.47988.

[76] E. Barjasteh, C. Sutanto, T. Reddy, J. Vinh, A graphene/graphite-based conductive polyamide 12 interlayer for increasing the fracture toughness and conductivity of carbon-fiber composites, Journal of Composite Materials 51 (20) (2017) 2879–2887. doi:10.1177/0021998317705707.

[77] Z. Zhao, G. Xian, J. Yu, J. Wang, J. Tong, J. Wei, C. Wang, P. Moreira, X. Yi, Development of electrically conductive structural BMI based CFRPs for lightning strike protection, Composites Science and Technology 167 (2018) 555–562. doi:10.1016/j.compscitech.2018.08.026.

[78] J. qian Xuan, D. sen Li, L. Jiang, Fabrication, properties and failure of 3d stitched carbon/epoxy composites with no stitching fibers damage, Composite Structures 220 (2019) 602–607. doi:10.1016/j.compstruct.2019.03.080.

[79] J. Rehbein, Conductivity improvement by using silver coated knitting yarn in ncf-reinforced laminates, ECCM 2017, Munch, Germany, 2016.

[80] K. A. Dransfield, L. K. Jain, Y.-W. Mai, On the effects of stitching in CFRPs—i. mode i delamination toughness, Composites Science and Technology 58 (6) (1998) 815–827. doi:10.1016/s0266-3538(97)00229-7.

[81] Y. Hirano, T. Yamane, A. Todoroki, Through-thickness electric conductivity of toughened carbon-fibre-reinforced polymer laminates with resin-rich layers, Composites Science and Technology 122 (2016) 67–72. doi:10.1016/j.compscitech.2015.11.018.

[82] J. Abry, In situ detection of damage in CFRP laminates by electrical resistance measurements, Composites Science and Technology 59 (6) (1999) 925–935. doi:10.1016/s0266-3538(98)00132-8.

[83] A. Todoroki, M. Tanaka, Y. Shimamura, Measurement of orthotropic electric conductance of CFRP laminates and analysis of the effect on delamination monitoring with an electric resistance change method, Composites Science and Technology 62 (5) (2002) 619–628. doi:10.1016/s0266-3538(02)00019-2.

[84] E. J. Garboczi, K. A. Snyder, J. F. Douglas, M. F. Thorpe, Geometrical percolation threshold of overlapping ellipsoids, Physical Review E 52 (1) (1995) 819–828. doi:10.1103/physreve.52.819.

[85] A. Oliva-Avilés, F. Avilés, G. Seidel, V. Sosa, On the contribution of carbon nanotube deformation to piezoresistivity of carbon nanotube/polymer composites, Composites Part B: Engineering 47 (2013) 200–206. doi:10.1016/j.compositesb.2012.09.091.

[86] H. Yang, X. Yao, L. Yuan, L. Gong, Y. Liu, Strain-sensitive electrical conductivity of carbon nanotube-graphene-filled rubber composites under cyclic loading, Nanoscale 11 (2) (2019) 578–586. doi:10.1039/c8nr07737a.

[87] G. Yang, L. Liu, Z. Wu, Improved strain sensing capability of nanocarbon free-standing buckypapers based strain gauges, Smart Materials and Structures 28 (6) (2019) 065009. doi:10.1088/1361-665x/ab147e.

[88] J. Eom, J.-S. Heo, M. Kim, J. H. Lee, S. K. Park, Y.-H. Kim, Highly sensitive textile-based strain sensors using poly(3,4-ethylenedioxythiophene):polystyrene sulfonate/silver nanowire-coated nylon threads with poly-l-lysine surface modification, RSC Advances 7 (84) (2017) 53373–53378. doi:10.1039/c7ra10722f.

[89] Y. Lu, J. Jiang, S. Yoon, K.-S. Kim, J.-H. Kim, S. Park, S.-H. Kim, L. Piao, High-performance stretchable conductive composite fibers from surface-modified silver nanowires and thermoplastic polyurethane by wet spinning, ACS Applied Materials & Interfaces 10 (2) (2018) 2093–2104. doi:10.1021/acsami.7b16022.

[90] H.-Y. Liu, H.-C. Hsieh, J.-Y. Chen, C.-C. Shih, W.-Y. Lee, Y.-C. Chiang, W.-C. Chen, Fabrication and application of highly stretchable conductive fiber-based electrode of epoxy/NBR electrospun fibers spray-coated with AgNW/PU composites, Macromolecular Chemistry and Physics 220 (4) (2018) 1800387. doi:10.1002/macp.201800387.

[91] S. Lee, S. Shin, S. Lee, J. Seo, J. Lee, S. Son, H. J. Cho, H. Algadi, S. Al-Sayari, D. E. Kim, T. Lee, Ag nanowire reinforced highly stretchable conductive fibers for wearable electronics, Advanced Functional Materials 25 (21) (2015) 3114–3121. doi:10.1002/adfm.201500628.

[92] Y. Qureshi, M. Tarfaoui, K. K. Lafdi, K. Lafdi, Real-time strain monitoring and damage detection of composites in different directions of the applied load using a microscale flexible nylon/ag strain sensor, Structural Health Monitoring (2019) 147592171986998doi:10.1177/1475921719869986.

[93] J. A. Rodríguez-González, C. Rubio-González, J. A. Soto-Cajiga, Piezoresistive response of spray-coated multiwalled carbon nanotube/glass fiber/epoxy composites under flexural loading, Fibers and Polymers 20 (8) (2019) 1673–1683. doi:10.1007/s12221-019-8711-8.

[94] R. J. Hart, Electrical resistance based damage modeling of multifunctional carbon fiber reinforced polymer matrix composites, Ph.D. thesis. doi:10.17077/etd.aqjxf6ie.

[95] T. N. Tallman, F. Semperlotti, K. Wang, Enhanced delamination detection in multifunctional composites through nanofiller tailoring, Journal of Intelligent Material Systems and Structures 26 (18) (2015) 2565–2576. doi:10.1177/1045389x15571387.

[96] L. Cheng, G. Y. Tian, Surface crack detection for carbon fiber reinforced plastic (CFRP) materials using pulsed eddy current thermography, IEEE Sensors Journal 11 (12) (2011) 3261–3268. doi:10.1109/jsen.2011.2157492.

[97] B. Haefner, D. Berger, Design, data analysis and measurement uncertainty evaluation of an eddy-current sensor array for in-process metrology of carbon fiber reinforced plastics, CIRP Annals 68 (1) (2019) 539–542. doi:10.1016/j.cirp.2019.04.091.

[98] Y. He, G. Tian, M. Pan, D. Chen, Impact evaluation in carbon fiber reinforced plastic (CFRP) laminates using eddy current pulsed thermography, Composite Structures 109 (2014) 1–7. doi:10.1016/j.compstruct.2013.10.049.

[99] Y. He, R. Yang, Eddy current volume heating thermography and phase analysis for imaging characterization of interface delamination in CFRP, IEEE Transactions on Industrial Informatics 11 (6) (2015) 1287–1297. doi:10.1109/tii.2015.2479856.

[100] R. Hughes, B. Drinkwater, R. Smith, Characterisation of carbon fibre-reinforced polymer composites through radon-transform analysis of complex eddy-current data, Composites Part B: Engineering 148 (2018) 252–259. doi:10.1016/j.compositesb.2018.05.007.

[101] M. A. Machado, K.-N. Antin, L. S. Rosado, P. Vilaça, T. G. Santos, Contactless high-speed eddy current inspection of unidirectional carbon fiber reinforced polymer, Composites Part B: Engineering 168 (2019) 226–235. doi:10.1016/j.compositesb.2018.12.021.

[102] G. Mook, R. Lange, O. Koeser, Non-destructive characterisation of carbon-fibre-reinforced plastics by means of eddy-currents, Composites Science and Technology 61 (6) (2001) 865–873. doi:10.1016/s0266-3538(00)00164-0.

[103] M. Pan, Y. He, G. Tian, D. Chen, F. Luo, Defect characterisation using pulsed eddy current thermography under transmission mode and NDT applications, NDT & E International 52 (2012) 28–36. doi:10.1016/j.ndteint.2012.08.007.

[104] Q. Yi, G. Tian, H. Malekmohammadi, J. Zhu, S. Laureti, M. Ricci, New features for delamination depth evaluation in carbon fiber reinforced plastic materials using eddy current pulse-compression thermography, NDT & E International 102 (2019) 264–273. doi:10.1016/j.ndteint.2018.12.010.

[105] W. Yin, P. Withers, U. Sharma, A. Peyton, Noncontact characterization of carbon-fiber-reinforced plastics using multifrequency eddy current sensors, IEEE Transactions on Instrumentation and Measurement 58 (3) (2009) 738–743. doi:10.1109/tim.2008.2005072.

[106] Z. Zeng, Q. Tian, H. Wang, S. Jiao, J. Li, Testing of delamination in multidirectional carbon fiber reinforced polymer laminates using the vertical eddy current method, Composite Structures 208 (2019) 314–321. doi:10.1016/j.compstruct.2018.10.027.

[107] D. Bian, B. R. Beeksma, D. J. Shim, M. Jones, Y. L. Yao, Interlaminar toughening of GFRP—part i: Bonding improvement through diffusion and precipitation, Journal of Manufacturing Science and Engineering 139 (7) (2017) 071010. doi:10.1115/1.4036126.

[108] X. Cheng, T. Yokozeki, L. Wu, J. Koyanagi, H. Wang, Q. Sun, The enhancement effect of carbon-based nano-fillers/polyaniline hybrids on the through-thickness electric conductivity of carbon fiber reinforced polymer, Composites Part A: Applied Science and Manufacturing 105 (2018) 281–290. doi:10.1016/j.compositesa.2017.12.002.

[109] X. Cheng, T. Yokozeki, L. Wu, H. Wang, J. Zhang, J. Koyanagi, Z. Weng, Q. Sun, Electrical conductivity and interlaminar shear strength enhancement of carbon fiber reinforced polymers through synergetic effect between graphene oxide and polyaniline, Composites Part A: Applied Science and Manufacturing 90 (2016) 243–249. doi:10.1016/j.compositesa.2016.07.015.

[110] G. Singer, G. Sinn, H. Rennhofer, R. Schuller, T. Grünewald, M. Unterlass, U. Windberger, H. Lichtenegger, High performance functional composites by in-situ orientation of carbon nanofillers, Composite Structures 215 (2019) 178–184. doi:10.1016/j.compstruct.2019.02.020.

[111] I. Gaztelumendi, M. Chapartegui, R. Seddon, S. Flórez, F. Pons, J. Cinquin, Enhancement of electrical conductivity of composite structures by integration of carbon nanotubes via bulk resin and/or buckypaper films, Composites Part B: Engineering 122 (2017) 31–40. doi:10.1016/j.compositesb.2016.12.059.

[112] Y. Lin, M. Gigliotti, M. C. Lafarie-Frenot, J. Bai, D. Marchand, D. Mellier, Experimental study to assess the effect of carbon nanotube addition on the through-thickness electrical conductivity of CFRP laminates for aircraft applications, Composites Part B: Engineering 76 (2015) 31–37. doi:10.1016/j.compositesb.2015.02.015.

[113] P. Latko-Durałek, K. Dydek, P. Bolimowski, E. Golonko, P. Durałek, R. Kozera, A. Boczkowska, Nonwoven fabrics with carbon nanotubes used as interleaves in CFRP, IOP Conference Series: Materials Science and Engineering 406 (2018) 012033. doi:10.1088/1757-899x/406/1/012033.

[114] K. Dydek, A. Boczkowska, P. Latko-Durałek, M. Wilk, K. Padykuła, R. Kozera, Effect of the areal weight of cnt-doped veils on cfrp electrical properties, Journal of Composite Materials 0 (0) (2020) 0021998320902227. arXiv:https://doi.org/10.1177/0021998320902227, doi:10.1177/0021998320902227.

[115] F. Pegorin, K. Pingkarawat, A. Mouritz, Controlling the electrical conductivity of fibre-polymer composites using z-pins, Composites Science and Technology 150 (2017) 167–173. doi:10.1016/j.compscitech.2017.07.018.

[116] J. Guo, Q. Zhang, L. Gao, W. Zhong, G. Sui, X. Yang, Significantly improved electrical and interlaminar mechanical properties of carbon fiber laminated composites by using special carbon nanotube pre-dispersion mixture, Composites Part A: Applied Science and Manufacturing 95 (2017) 294 – 303. doi:https://doi.org/10.1016/j.compositesa.2017.01.021.

***conflict of Interest Statement**

Declaration of interests

☒ The authors declare that they have no known competing financial interests or personal relationships that could have appeared to influence the work reported in this paper.

☐The authors declare the following financial interests/personal relationships which may be considered as potential competing interests: